Using Detailed Single-star and Binary-evolution Models to Probe the Large Observed Luminosity Spread of Red Supergiants in Young Open Star Clusters

Chen Wang[1] , Lee Patrick[2] , Abel Schootemeijer[3] , Selma E. de Mink[1] , Norbert Langer[3] , Nikolay Britavskiy[4,5] ,
Xiao-Tian Xu[3] , Julia Bodensteiner[6,7] , Eva Laplace[8] , Ruggero Valli[1] , Alejandro Vigna-Gómez[1] , Jakub Klencki[1,6] ,
Stephen Justham[1] , Cole Johnston[1] , and Jing-ze Ma[1]

[1] Max Planck Institute for Astrophysics, Karl-Schwarzschild-Strasse 1, 85748 Garching, Germany; cwang@mpa-garching.mpg.de
[2] Departamento de Astrofísica, Centro de Astrobiología, (CSIC-INTA), Ctra. Torrejón a Ajalvir, km 4, 28850 Torrejón de Ardoz, Madrid, Spain
[3] Argelander-Institut für Astronomie, Universität Bonn, Auf dem Hügel 71, 53121 Bonn, Germany
[4] Université de Liège, Quartier Agora (B5c, Institut d'Astrophysique et de Géophysique), Allée du 6 Août 19c, 4000 Sart Tilman, Liège, Belgium
[5] Royal Observatory of Belgium, Avenue Circulaire/Ringlaan 3, 1180 Brussels, Belgium
[6] European Southern Observatory, Karl-Schwarzschild-Str. 2 85738 Garching bei München, Germany
[7] Anton Pannekoek Institute for Astronomy, University of Amsterdam, Postbus 94249, 1090GE Amsterdam, The Netherlands
[8] Heidelberger Institut für Theoretische Studien, Schloss-Wolfsbrunnenweg 35, D-69118 Heidelberg, Germany
Received 2025 January 14; revised 2025 February 6; accepted 2025 February 14; published 2025 February 27

Abstract

Red supergiants (RSGs) represent a late evolutionary stage of massive stars. Recent observations reveal that the observed luminosity range of RSGs in young open clusters is wider than expected from single-star evolution models. Binary evolution effects have been suggested as a possible explanation. Here, we analyze 3670 detailed binary-evolution models, as well as corresponding single-star models, to probe the contribution of binary mass transfer and binary mergers to the luminosity distribution of RSGs in star clusters with ages up to 100 Myr. We confirm that the expected luminosity range of RSGs in a coeval population can span a factor of 10, as a consequence of mergers between two main-sequence stars, which reproduces the observed RSG luminosity ranges in rich clusters well. While the luminosity increase as consequence of mass transfer is more limited, it may help to increase the number of overluminous RSGs. However, our results also demonstrate that binary effects alone are insufficient to account for the number of RSGs found with luminosities of up to 3 times those predicted by current single-star models. We discuss observational accuracy, rotational mixing, age spread, and intrinsic RSG variability as possible explanations. Further observations of RSGs in young open clusters, in particular studies of their intrinsic brightness variability, appear crucial for disentangling these effects.

Unified Astronomy Thesaurus concepts: Red supergiant stars (1375); Young star clusters (1833); Binary stars (154); Massive stars (732); Red straggler stars (1374); Stellar evolution (1599); Stellar evolutionary models (2046)

Materials only available in the online version of record: animation

1. Introduction

Red supergiants (RSGs) are cool giant massive stars that represent a late phase of stellar evolution, where the star has exhausted hydrogen in its core and is now fusing heavier elements. They are considered progenitors of hydrogen-rich Type II-P supernovae (SNe). Understanding the formation and evolution of RSGs is crucial for advancing our knowledge of stellar evolution and the chemical yields from SN explosions. Despite their importance, key processes governing RSG formation and evolution, such as the roles of stellar rotation and binary interaction, remain poorly constrained.

It is widely accepted that massive stars are primarily born with close companions (H. Sana et al. 2012; S. S. R. Offner et al. 2023). Studies have shown that binary evolution significantly alters the luminosity of RSGs (J. J. Eldridge et al. 2008, 2020; E. Zapartas et al. 2019; F. R. N. Schneider et al. 2024). Young open clusters provide an excellent laboratory for studying these effects, as their coeval stellar populations would produce similar luminosities among RSGs if only single-star evolution were at play. Using BPASS single and binary models, J. J. Eldridge et al. (2020) demonstrated that binary evolution can greatly

extend the luminosity distribution of RSGs in young star clusters. Mergers and mass accretors can appear more luminous than other RSGs, whereas RSGs undergoing mass transfer may have lower luminosities. In fact, recent high-quality spectroscopic observations reveal that the luminosity distribution of RSGs in young open clusters is too broad to be explained by single-star evolution (N. Britavskiy et al. 2019; L. R. Patrick et al. 2020). The more luminous RSGs, known as "red stragglers," appear younger and more massive than their counterparts and are thought to be results of binary evolution.

From another point of view, based on the analysis of large numbers of detailed binary models, our previous studies (C. Wang et al. 2020, 2022) show that binary evolution is crucial in explaining the extended main-sequence (MS) turnoff in young open clusters observed by the Hubble Space Telescope over the past decade (A. P. Milone et al. 2009, 2015, 2018, 2023; C. Li et al. 2017). We proposed that MS mergers (mergers between two MS stars) produce hot and luminous blue stragglers, whereas stable mass transfer mainly results in fast-rotating Be stars that are cooler than other MS stars in the cluster. These MS stars are expected to exhibit distinct properties during later stages, such as the RSG phase. For instance, blue stragglers are expected to evolve into red stragglers as they progress through their evolution.

Previous studies have suggested that RSGs are unique indicators of cluster age (E. R. Beasor et al. 2019; N. Britavskiy et al. 2019;

J. J. Eldridge et al. 2020), especially given the fact that the MS turnoff is usually extended in young open clusters (A. P. Milone et al. 2018, 2023). While some studies argue that the least luminous RSGs are ideal age indicators, since more luminous red stragglers are likely binary products (E. R. Beasor et al. 2019; N. Britavskiy et al. 2019), others suggest that the mean luminosity of all RSGs provides a better measure, as this value is similar in both single and binary evolution (J. J. Eldridge et al. 2020). Thus, understanding the influence of binary interaction on RSGs is essential for accurately using them as age indicators.

In this study, we investigate the RSG phase of our detailed binary models from C. Wang et al. (2022), offering the first comprehensive analysis of RSGs in young open clusters based on a large set of detailed binary models. Compared to the BPASS models used in J. J. Eldridge et al. (2020), our models evolve both stars simultaneously and include the spin-up of accretors. Our models also treat mass transfer stability and efficiency in a self-consistent approach. Furthermore, compared to J. J. Eldridge et al. (2020), who focused solely on the luminosity spread of RSGs without considering the time they spend at each luminosity, our study provides a comprehensive population synthesis analysis of the luminosity distribution and number of RSGs from various evolutionary pathways.

We compare our results with observed RSGs in four young open clusters, NGC 330 (L. R. Patrick et al. 2020) in the Small Magellanic Cloud (SMC) and NGC 2004, NGC 2100, and NGC 1818 (E. R. Beasor & B. Davies 2016; E. R. Beasor et al. 2019; N. Britavskiy 2024, private communication) in the Large Magellanic Cloud (LMC). We aim to enhance our understanding of the properties of RSGs originating from different pathways and provide useful constraints on massive binary evolution. We select these four clusters to study because they are in Magellanic Clouds; thus, from the observational point of view, there is less extinction, and as a result, the luminosity estimates are more reliable for RSGs in these clusters (the luminosity estimates are mainly from the K-band photometry). While other clusters with RSGs are known in the Galaxy (see Table 1 in J. J. Eldridge et al. 2020), their luminosity estimates (and spread) are less robust due to uncertain extinction around RSGs, especially in very crowded regions in the Galaxy. Therefore, studying RSGs in Magellanic Cloud clusters provides a more secure basis for our analysis than studying those in the Galaxy.

This Letter is structured as follows. In Section 2, we introduce our detailed single and binary models. In Section 3, we demonstrate the predicted properties of RSGs in young open clusters from both single-star and binary evolution and compare with recent observations. Then we discuss the impact of uncertainties on our results in Section 4 and summarize our conclusions in Section 5.

2. Models and Physics Assumptions

2.1. Detailed Single-star Models

We first explore whether the observed RSGs in four young open clusters can be explained by single-star evolution. For this purpose, we employ single-star models computed by B. Hastings et al. (2021) using the MESA code (version 12115; B. Paxton et al. 2011, 2013, 2015, 2018). These models cover initial masses ranging from 2 to $20\,M_\odot$. We extended these models up to initial masses of $100\,M_\odot$, with a mass interval of $\log m_i = 0.04$. These models adopt physics assumptions nearly identical to those in A. Schootemeijer et al. (2019),
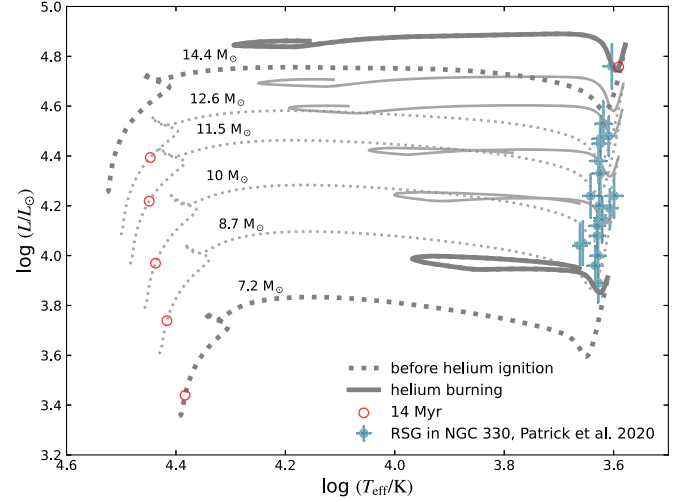
Figure 1. Comparison of observed RSGs (cyan dots with error bars) in the SMC cluster NGC 330 (L. R. Patrick et al. 2020) with the evolution of our nonrotating single-star models (gray lines) in the HRD. Initial stellar masses are indicated along the tracks. The lower and upper thick tracks represent the best fits for the least luminous and most luminous RSGs observed in NGC 330, respectively. Solid gray lines denote the helium-burning stages of the stellar models, while dotted lines indicate the stages before helium ignition. Here we define the helium-burning phase as the period during which the central helium mass fraction ranges from 0.98 and 0.001. The red circles indicate the positions of the stellar models at 14 Myr for each mass.

except for a mass-dependent overshooting parameter. Specifically, $\alpha_{OV} = 0.3$ is used for stars with initial masses above $20\,M_\odot$ (I. Brott et al. 2011). Below $20\,M_\odot$, α_{OV} decreases linearly, reaching 0.1 at an initial mass of $1.66\,M_\odot$ (A. Claret & G. Torres 2016). Semiconvective mixing is set to $\alpha_{SC} = 10$ (A. Schootemeijer et al. 2019). The evolution starts from the zero-age MS (ZAMS) and terminates when core helium is depleted. We identify RSGs as stellar models with $T_{eff} < 4800$ K (M. R. Drout et al. 2009).

We consider both LMC and SMC metallicities. For direct comparison with observed RSGs (in Figures 1 and A2), we use nonrotating star models. Additionally, we employ rotating star models with the same physics assumptions for two parts in this work. First, we use stellar models initially rotating at 15% of their critical values to follow the evolution of MS merger products in our detailed binary models. Second, in our semianalytical method to calculate the upper luminosity limit of RSGs in young open clusters (see Section 3.2.2 and Appendix D for details), we employ single-star models with an initial rotation of 55% of their critical velocity for premerger stars. These two rotational velocities are chosen based on the findings of C. Wang et al. (2022), which suggest that most stars are likely born with around 55% of their critical rotational velocity, contributing to the major (red) MS in young open clusters. Binary merger products, if rotating at approximately 15% of their critical velocity, can explain the blue MS observed in these clusters.

2.2. Detailed Binary Models

We use the MESA detailed binary models[9] with the SMC metallicity in C. Wang et al. (2022, 2024). The initial binary parameters are created from Monte Carlo sampling. The initial

---

[9] We use MESA version 8845 to compute the binary models. The inlist files used for these computations can be found at Zenodo (https://zenodo.org/records/5233209).

primary masses are from 3 to $100\,M_\odot$ adopting the E. E. Salpeter ([1955](#)) initial mass function (IMF). The initial mass ratios range from 0.1 to 1, following a flat distribution (H. Sana et al. [2012](#); T. Shenar et al. [2022](#)). The initial orbital periods are from the minimum value, where the two stellar components are initially in contact, to 8.6 yr ($\log P_i\,/\mathrm{day} = 3.5$), assuming a flat distribution in logarithmic space (E. Öpik [1924](#); H. A. Abt [1983](#); G. Banyard et al. [2023](#)). We simulate the evolution of 3670 detailed binary systems, representing clusters with an initial total stellar mass of approximately $1.3 \times 10^5\,M_\odot$, under the assumption of a 100% binary fraction and a lower mass limit of $0.08\,M_\odot$ (see C. Wang et al. [2024](#) for details).

The adopted upper period limit of $\log P = 3.5$ reliably reaches the noninteraction region for binaries with primary masses lower than approximately $25\,M_\odot$ (whose MS lifetime is around 7.6 Myr). However, the true upper period limit for binaries remains unclear, especially in dense environments such as star clusters, where dynamical evolution is expected to disrupt wide systems (C. Korntreff et al. [2012](#)). For the lower period limit, we use the period at which the two stars are initially in contact at the ZAMS. Binaries that are not initially in contact but where the primary star fills its Roche lobe at the ZAMS phase are classified as ZAMS mergers. We assume that ZAMS merger products are also ZAMS stars. The fraction of ZAMS mergers, as well as similar populations of stars including pre-MS mergers and mergers occurring before and shortly after the ZAMS phase, remains uncertain. C. Wang et al. ([2022](#)) proposed that a substantial fraction of binaries (between 10% and 30%) must merge within the first 1–2 Myr to account for the observed ratio of MS stars on the double MSs in young open clusters. Similarly, recent simulations on binary formation suggest that a significant fraction of early mergers (or even pre-MS mergers) occurs in B-type binaries, with estimates as high as 30% (A. Tokovinin & M. Moe [2020](#)).

All stellar models are assumed to rotate at 55% of their critical velocities at the ZAMS. This choice is motivated by the need to explain the major (red) MS stars in young star clusters (C. Wang et al. [2022](#)).

The same physics used for the single-star models is applied to our binary models. Binary evolution begins at the ZAMS with circular orbits, and mass and angular momentum are transferred via Roche-lobe overflow (R. Kippenhahn & A. Weigert [1967](#); S. E. de Mink et al. [2013](#)). We account for the spin-up of accretors during mass transfer (W. Packet [1981](#)), assuming that once an accretor reaches critical rotation, further accretion is halted. This results in accretion efficiency being dependent on the binary's orbital period, with values below a few percent in long-period Case B binaries and reaching up to 60% in short-period Case A binaries (C. Wang et al. [2022](#); K. Sen et al. [2022](#)).

The excess material that cannot be accreted by the accretor is then assumed to be expelled from the stellar surface, driven by the combined radiation energy of both stars. If this radiation energy is insufficient to expel the material, we assume the two stars merge. Mergers are also assumed when mass is lost through the second Lagrangian point or when the mass transfer rate exceeds an ad hoc upper limit of $\log \dot{M} > 10^{-1}\,M_\odot\,\mathrm{yr}^{-1}$, indicating unstable mass transfer.

We use the method in F. R. N. Schneider et al. ([2016](#)) to calculate the evolution of merger products from two MS stars, assuming that the merger products have an initial rotational velocity of 15% of their critical value. We do not model the evolution of merger products involving a post-MS star, as no well-established models currently exist. Previous studies suggest that such mergers are likely to ignite helium as blue supergiants (BSGs) or yellow supergiants (YSGs; P. Podsiadlowski [1992](#); S. Justham et al. [2014](#)) and may stay blue for most of their remaining lifetimes. We discuss this omission in Section [4.4.3](#).

If none of the previously mentioned merger criteria are met, we follow the evolution of the binary models until core carbon exhaustion in both components. For numerical stability reasons, we limit the calculations to central helium exhaustion if the helium core mass exceeds $13\,M_\odot$. In some noninteraction binaries, the primary star encounters convergence issues during its asymptotic giant branch (AGB) evolution. For these cases, we terminate the evolution of the primary star at the end of helium exhaustion and allow the secondary star to continue evolving in isolation.

If the final core mass of the primary star surpasses the Chandrasekhar limit at carbon/helium depletion, we assume a compact object formation, after which the companion is modeled as an isolated star. It is important to note that our simulations do not account for the impact of SN kicks. Our simulations represent the case in which binaries are disrupted due to the SN kick, with the secondary star remaining in the cluster as a single star. We discuss the impact of SN kicks in Section [3.2.4](#) and Appendix [G](#).

3. Results

3.1. Single-star Models Fail to Explain Observations

In a star cluster comprised solely of coeval, nonrotating single stars, RSGs are expected to originate from stars with similar initial masses. Given the small luminosity variation of single stars during the helium-burning phase, the luminosity distribution of RSGs in a star cluster resulting from single-star evolution is anticipated to be narrow. However, recent spectroscopic observations of RSGs in young open clusters reveal a significantly broader luminosity range than predicted by single-star evolution (E. R. Beasor et al. [2019](#); N. Britavskiy et al. [2019](#)), based on Brott models (I. Brott et al. [2011](#)) and MIST models (J. Choi et al. [2016](#)).

Using the SMC cluster NGC 330 (L. R. Patrick et al. [2020](#)) as an example, we compare the distribution of its RSGs with the evolutionary tracks from our MESA single-star models in the Hertzsprung–Russell diagram (HRD) in Figure [1](#). It is evident that the observed luminosity spread of RSGs cannot be accounted for by one single-star track. Notably, the most luminous RSG requires a model nearly twice as massive as the least luminous one. Based on these models, the estimated ages of the least and most luminous RSGs are around 40 Myr and 14 Myr, respectively. This challenges our traditional understanding of star clusters that all stars are coeval. At 14 Myr, stars below $14\,M_\odot$ are still on their MS evolution. This indicates that the more massive, "younger" RSGs should have experienced rejuvenation to remain observable as RSGs at a similar age as the less massive star. Rejuvenation refers to a process in which a star appears younger than it actually is, primarily due to mechanisms that either mix fresh fuel into the core or simultaneously increase the star's total mass, thereby shortening its MS lifetime. The first scenario includes rotationally induced mixing (A. Maeder & G. Meynet [2000](#);
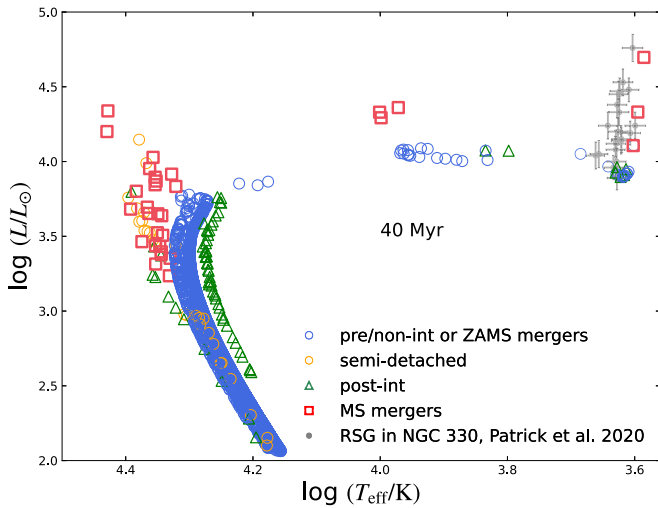
Figure 2. Distribution of our detailed binary models in the HRD at 40 Myr. Each open marker indicates the visually brighter component of a binary system. Blue circles represent binaries that have not yet begun to interact or will never interact. Orange circles denote stars currently undergoing nuclear-timescale mass accretion. Green triangles mark stars that have experienced stable mass transfer. Red squares depict the products of mergers of two MS stars. For comparison, we have superimposed the observed RSGs in NGC 330, shown with gray dots with error bars. This figure is a snapshot from an animation illustrating the distribution of our models from 2 to 100 Myr. The animation is designed with a black background for enhanced visibility during presentation and has a duration of 27 s. The brown shaded area in the animation highlights the region where we identify RSGs.

(An animation of this figure is available in the online article.)

S. E. de Mink et al. 2009), while the second includes binary mass transfer and binary mergers (S. Neo et al. 1977; P. Hellings 1983; F. R. N. Schneider et al. 2016).

Our single-star models do not include the AGB phase. By analyzing our noninteraction binaries that successfully evolve through this phase, we found that the probability of having an AGB star that is 0.5 dex more luminous than the least luminous RSG in a star cluster is less than approximately 2% (see Figure A3). Therefore, AGB stars are unlikely to account for the observed luminosity spread of RSGs in young open clusters. Nonetheless, in rare cases, AGB stars can contaminate the red straggler population, as shown in our animation (e.g., see 26.86 Myr).

The same result that the observed luminosity spread cannot be explained by single-star evolution is also found for RSGs in three LMC clusters, NGC 2004, NGC 2100, and NGC 1818 (see Figure A2).

3.2. Predictions from Binary Models and Comparisons with Observations

3.2.1. Distribution in the HRD

In the following, we explore how binary evolution impacts the properties of RSGs in young open clusters. We show the distribution of our detailed binary models in the HRD at an age of 40 Myr, alongside the observed RSGs in NGC 330 (L. R. Patrick et al. 2020) in Figure 2. This age was selected because the luminosities of both the least and most luminous RSG models match the observations well, and it aligns with the age derived from the MS turnoff of this cluster (C. Wang et al. 2022).

RSGs originating from pre/noninteraction binaries, as well as ZAMS mergers, evolve similarly to single stars. In this work, RSGs from preinteraction binaries specifically refer to those that will undergo Case C mass transfer after helium exhaustion, which we assume to be unstable and lead to mergers. RSGs in preinteraction binaries are primarily the primary stars in these binaries, while RSGs in noninteraction binaries can originate from either the primary or the secondary star. As anticipated, RSGs originating from these scenarios exhibit comparable luminosities, representing the least luminous subset of the RSG population.

In our simulations, RSGs formed from stable mass transfer exhibit similar luminosities to those from pre/noninteraction binaries. The reason is that the vast majority of these RSGs are accretors that have undergone Case B mass transfer (see the right panel of Figure B2 for an evolutionary example), during which they accrete only tiny amounts of material. As a result, neither their total mass nor core mass increase significantly, leading to minimal rejuvenation. On the other hand, accretors in Case A mass transfer (see the left panel of Figure B2 for an evolutionary example) can accrete more material, leading to a substantial increase in both their total and core masses, resulting in stronger rejuvenation. However, due to the presence of a composition gradient above the convective core, and given our assumptions on internal mixing, the accretor cannot undergo complete rejuvenation, where its core mass fully grows to match that of a genuinely single star with the same total mass. Instead, the accretor experiences incomplete rejuvenation, meaning it retains a smaller core compared to a genuinely single star of equivalent total mass. As shown in the left panel of Figure B2, such an accretor ignites helium and explodes as a BSG or YSG (see also H. Braun & N. Langer 1995; E. J. Farrell et al. 2019).

Figure 2 demonstrates that, in our simulations, nearly all high-luminosity RSGs (i.e., red stragglers) are from MS mergers. MS merger products manifest as blue stragglers during their MS evolution, appearing younger and more massive than the MS turnoff stars. These blue stragglers will similarly appear younger and more massive than typical RSGs and appear as red stragglers when they evolve into the RSG phase. The more massive the MS merger product, the higher the luminosity it will have during its RSG phase. It can be seen that our binary models closely reproduce the observed luminosity spread of RSGs in NGC 330. This means that the observed luminosity of red stragglers can be explained by MS merger origin.

Figure 2 also shows that we predict a luminosity spread among BSGs, with MS merger products exhibiting higher luminosities. Notably, this spread has been observed in BSGs in young open clusters (A. P. Milone et al. 2018). A detailed comparison between the predicted and observed properties of BSGs is beyond the scope of this study.

We present an animation that illustrates the distribution of RSGs in the HRD up to 100 Myr, with Figure 2 capturing a specific snapshot from this sequence.

3.2.2. Luminosity of RSGs Originating from MS Mergers

As shown in Figure 2, our MS merger models successfully reproduce the observed luminosity extension of RSGs in NGC 330. In this section, we examine more generally the RSG luminosity extension that MS mergers can generate in young open clusters up to 100 Myr and compare this with
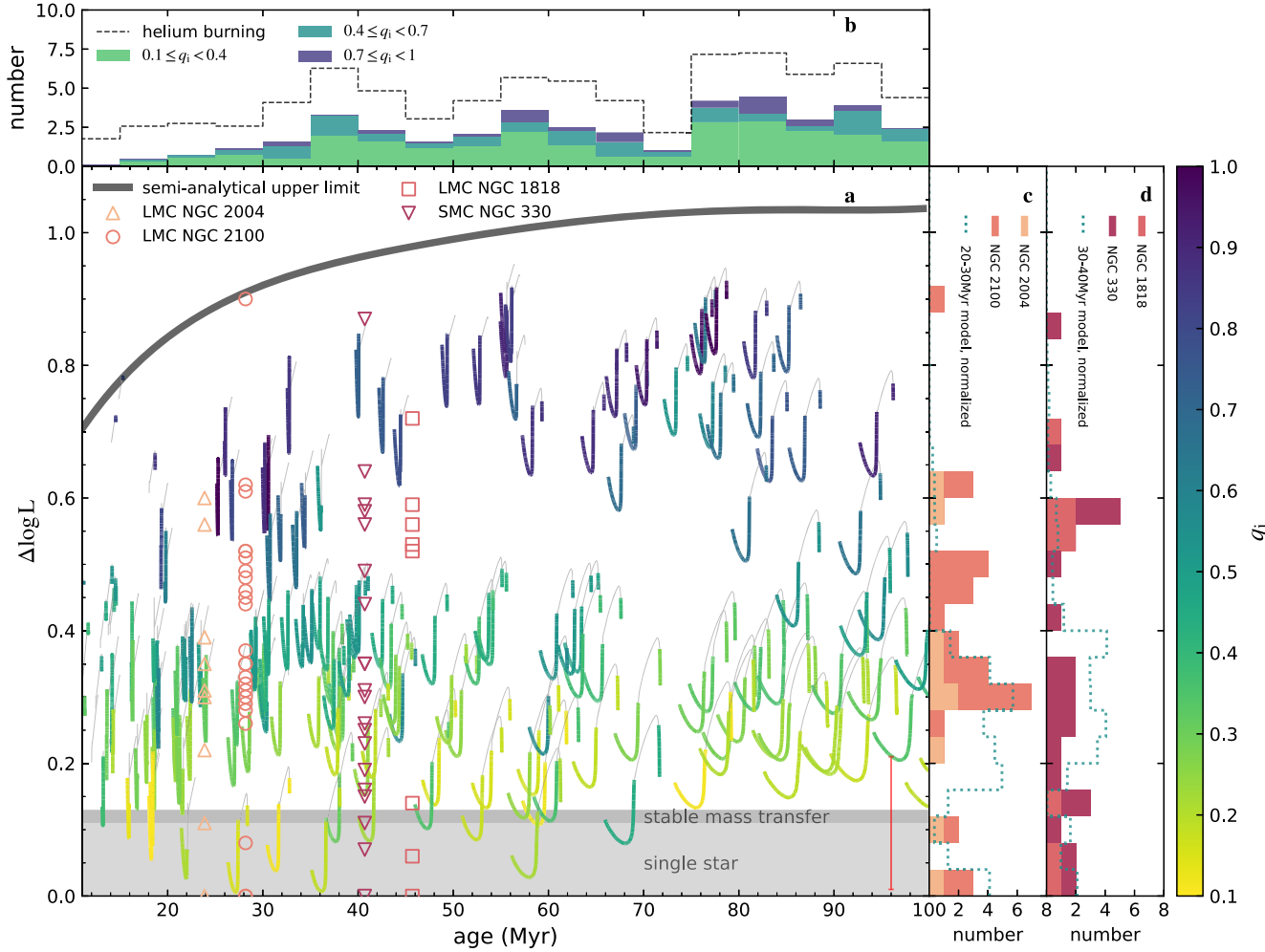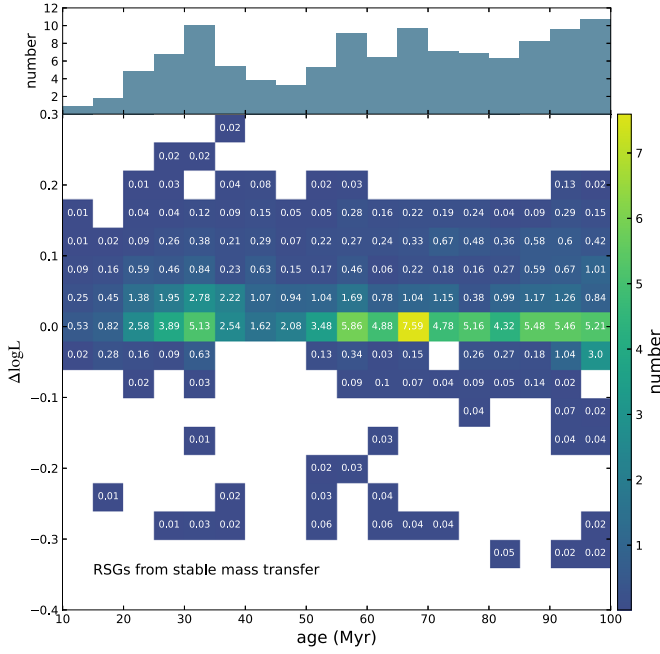
Figure 3. Panel (a): the luminosity extension $\Delta \log L = \log L - \log L_0$ for RSGs originating from MS mergers in our simulations as a function of age, where L is the luminosity of RSGs and L_0 is the baseline luminosity (see Appendix C). Each track represents the luminosity variation for one RSG, with color indicating the initial mass ratio q_i (defined as the ratio of the secondary star's mass to the primary star's mass) of its binary progenitor (see the color bar on the right side of the figure). Thin gray lines along the tracks indicate periods when the corresponding MS merger model is in the BSG or YSG phase. The thick dark gray curve represents results from the semianalytical approach, where we assume that mergers happen between two MS turnoff stars (see Appendix D). Light and dark gray shaded areas indicate the range of $\Delta \log L$ predicted by single-star evolution and stable mass transfer, respectively. These ranges are determined to encompass 95% of the RSGs produced in these two scenarios. Open markers illustrate the luminosity difference for each observed RSG relative to the least luminous RSG in its cluster, with cluster ages determined by comparing this least luminous RSG with our single-star models (see Figure C1). The red error bar in the lower right corner of this panel represents the observational uncertainty (± 0.1 dex). Panel (b): the number distribution of RSGs in clusters with a total initial mass of $1.3 \times 10^5 \, M_\odot$ originating from MS mergers as a function of age. Models are categorized into three groups based on the initial mass ratios of the merger progenitors. The bars are stacked. The black dashed steps indicate the predicted number distribution for the helium-burning stars, i.e., including RSGs, BSGs, and YSGs. Panel (c): $\Delta \log L$ distribution for the observed RSGs in clusters NGC 2004 (light orange bars) and NGC 2100 (orange bars). The bars are stacked. The green dashed steps depict the predicted $\Delta \log L$ distribution for our MS merger models between 20 and 30 Myr, normalized to match the total number of observed RSGs in these two clusters. Panel (d): same as panel (c) but for observed RSGs in clusters NGC 1818 (light red bars) and NGC 330 (dark red bars). And the green dashed steps represent the predicted $\Delta \log L$ distribution for our models between 40 and 50 Myr.

observational data. The results are shown in Figure 3. Here $\Delta \log L = \log L - \log L_0$ represents the difference in logarithmic space between the luminosity of RSGs in our binary merger models (L) and the reference luminosity (L_0) derived from single-star models at a given cluster age. The definition of L_0 is explained in detail in Appendix C. Briefly, we use the weighted mean luminosity of single-star models during their RSG evolution as the baseline luminosity.

Each track in panel (a) represents the evolution of one RSG model. The changes in $\Delta \log L$ result from two combined effects: (1) the decrease of $\log L_0$ with age and (2) the luminosity evolution during the RSG phase. For reference, we also indicate the range of $\Delta \log L$ predicted by our models for RSGs originating from single-star evolution (light gray shaded area) and stable mass transfer (dark gray shaded area). To

determine this, we analyze the results in Figures 4 and A4 and calculate the range of $\Delta \log L$ encompassing 95% of RSGs from these scenarios. Our analysis shows a range of -0.03 to 0.11 (a spread of 0.14 dex) for scenarios resembling single-star evolution and -0.05 to 0.13 (a spread of 0.18 dex) for stable mass transfer. Accordingly, the boundaries of the light and dark gray shaded areas are set to 0.11 and 0.13, respectively. It can be seen that MS mergers produce RSGs with a significantly broader luminosity distribution compared to those produced by single-star evolution or stable mass transfer.

We notice that our simulations are limited to a single set of initial parameters and therefore cannot fully represent all star clusters. To remedy this, we provide a semianalytical analysis to establish the upper limit for $\Delta \log L$ of RSGs originating from MS mergers (see Appendix D for more details). The idea

Figure 4. Predicted luminosity extension $\Delta \log L = \log L - \log L_0$ for RSGs originating from stable mass transfer as a function of age. The color scale indicates the predicted number of RSGs in clusters with a total initial mass of $1.3 \times 10^5 \, M_\odot$ produced through stable mass transfer. The exact value in each pixel is labeled. 1D projections of the distribution are displayed in the top panel.

is that the most luminous (and massive) red straggler in a cluster was previously the most luminous (and massive) blue straggler, which should have formed through the merger of two turnoff stars. The results are shown by the thick solid gray curve in panel (a) of Figure 3. We predict an upper limit of 0.8–1.0 dex for the luminosity extension of RSGs in clusters aged between 15 and 100 Myr. RSGs originating from MS mergers are not expected to exceed this luminosity limit.

In panel (a) of Figure 3, we overplot observational data from four young open clusters, with $\Delta \log L$ representing the luminosity difference between each observed RSG and the least luminous RSG within the same cluster in the logarithmic space. The cluster ages are determined by comparing the luminosity of the least luminous RSG in each cluster with the relationship between L_0 and cluster age predicted by single-star models (see the orange lines in Figure C1). Since metallicity has a negligible impact on the relationship between L_0 and cluster age, it is reasonable to compare observations from both the LMC and SMC with our SMC binary models. It can be seen that the luminosities of all observed RSGs fall within the predicted range, indicating that the observed high-luminosity red stragglers can be effectively explained by the MS merger scenario.

Panel (b) shows the number distribution of RSGs originating from MS mergers, as predicted by our simulations, grouped by the initial mass ratios of the merger progenitors. The number in each age bin is calculated as

$$N = \sum_i \frac{t_i}{t_{\rm bin}}, \qquad (1)$$

where i represents the index of each RSG, t_i denotes the time the ith RSG spends in this age bin, and $t_{\rm bin} = 5$ Myr is the

width of the age bin. It can be seen that the predicted number of RSGs does not vary significantly with age. On one hand, the influence of the IMF would suggest a higher number of RSGs in older clusters. On the other hand, the parameter space for MS mergers decreases with lower primary masses (see Figure B1), and the mass range of RSGs within a constant age bin also narrows over time.

In panels (c) and (d), we present the $\Delta \log L$ distribution for the observed RSGs, divided into two age groups. We also show the predicted $\Delta \log L$ distributions of RSGs originating from MS mergers for the specific age ranges indicated in the figure legend. These distributions are normalized such that the total number of predicted RSGs matches the number of observed RSGs in each panel. It is important to note that we do not intend to directly compare our model predictions with the observations here, as the predictions include only MS merger products. If contributions from scenarios resembling single-star evolution were included, a significant peak at $\Delta \log L \lesssim 0.1$ (see Figure A4) would be expected. A comparison that accounts for RSGs from other evolutionary scenarios is provided in Figure 5. Here, we focus solely on the $\Delta \log L$ distribution of RSGs from MS mergers.

Our predictions align with observational data in that the majority of RSGs exhibit relatively low luminosities ($\Delta \log L \lesssim 0.4$ in our predictions, compared to $\Delta \log L \lesssim 0.6$ in observations). In our simulations, lower-mass-ratio binaries are more likely to merge than higher-mass-ratio binaries, leading to a prediction of more lower-luminosity RSGs than higher-luminosity RSGs originating from the MS merger scenario. The discrepancy between the predicted peak at $0.2 \lesssim \Delta \log L \lesssim 0.4$ and the significant fraction of observed RSGs with $0.4 \lesssim \Delta \log L \lesssim 0.6$ may be explained by observational errors (± 0.1 dex), photometric variability, and the accuracy of the measurement of the least luminous RSG in these clusters. We will discuss this in detail in Section 4.2.

3.2.3. Luminosity of RSGs Originating from Stable Mass Transfer

In Figure 4, we display the predicted $\Delta \log L$ for RSGs originating from stable mass transfer across different cluster ages. Unlike Figure 3, here we use the heat plot and display the predicted number of RSGs in each pixel, because RSGs originating from stable mass transfer have a much narrower $\Delta \log L$ distribution and a larger number, such that all tracks like those in Figure 3 will accumulate at $\Delta \log L \sim 0$. The number in each pixel is calculated using Equation (1). It is important to note that in our standard simulations, we assume that the secondary star evolves in isolation and remains in the cluster after the primary star evolves to a compact object.

Consistent with Figure 2, Figure 4 demonstrates that the luminosity extension of the RSGs originating from stable mass transfer is small due to low mass transfer efficiency, with 95% having $\Delta \log L$ between -0.05 and 0.13 (0.18 dex spread). RSGs with $\Delta \log L \lesssim -0.1$ are those before helium ignition and are unlikely to have significant observational consequences (see also Figure A4).

3.2.4. Number of RSGs and Fraction of Red Stragglers

In Figure 5, we show the predicted number of RSGs in clusters with initial stellar masses of $1.3 \times 10^5 \, M_\odot$ arising from different evolutionary scenarios. The number is calculated using the same method as that in panel (b) of Figure 3.
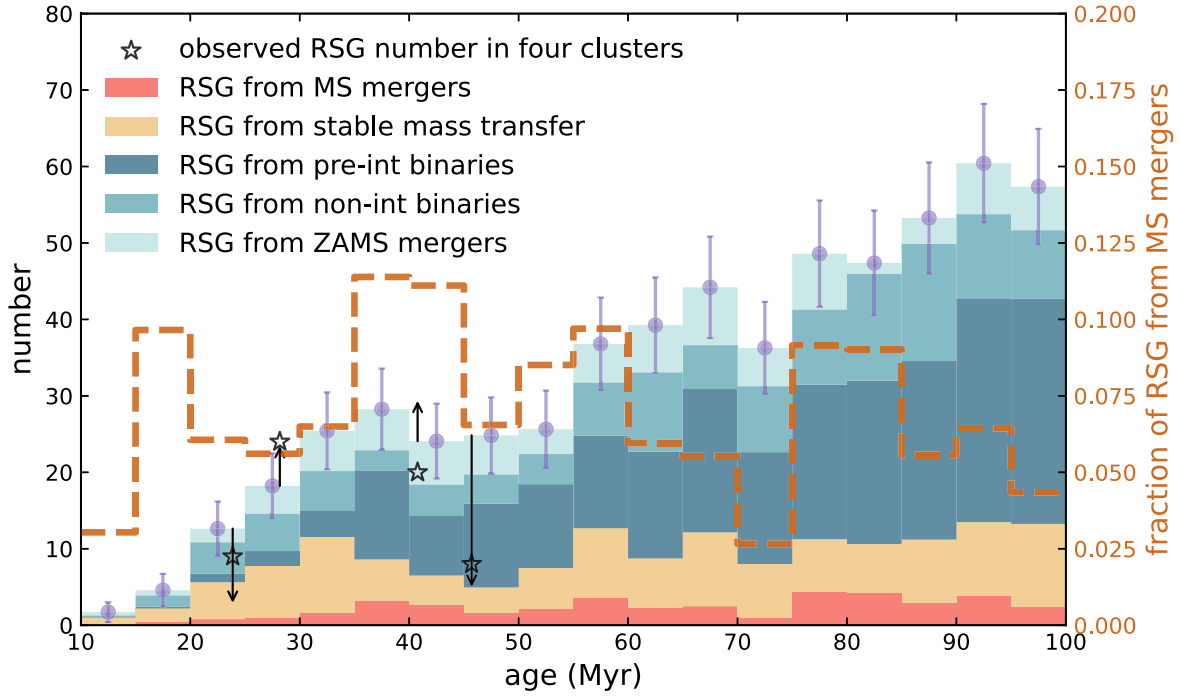
Figure 5. Number of RSGs in clusters with an initial total mass of $1.3 \times 10^5 M_\odot$ from different evolutionary scenarios predicted by our detailed binary models. Orange-red bars represent RSGs originating from MS mergers. Yellow bars depict RSGs resulting from stable mass transfer without taking into account SN kicks. Dark blue and medium blue bars represent RSGs that have not interacted with their companions or will never interact, respectively. Light blue bars correspond to RSGs from ZAMS mergers. The bars are stacked to provide a cumulative representation. Purple dots with error bars indicate the standard deviation of the total number of RSGs predicted in our simulations. Open pentagrams show the observed number of RSGs in clusters NGC 2004, NGC 2100, NGC 330, and NGC 1818, displayed from left to right. The endpoints of the black arrows show the predicted number of RSGs for each cluster, adjusted according to their total masses (see the text for details). The brown dashed steps illustrate the fraction of RSGs from MS mergers relative to the total number of RSGs in our simulation (i.e., the value predicted by the orange-red bars divided by the sum of all five populations). The corresponding values are shown on the right y-axis.

It can be seen that the number of RSGs from pre/noninteraction binaries increases with cluster age, due to the IMF and the increasing parameter space for non/preinteraction systems (see Figure B1). In contrast, the number of RSGs formed from stable mass transfer and MS mergers remains relatively constant with cluster age. As previously explained, the effect of the IMF is balanced by the shrinking parameter space for these evolutionary pathways.

To compare our predicted numbers with observational data, we scale the predictions by the ratio of the observed cluster mass to the simulated mass ($1.3 \times 10^5 M_\odot$). The scaled results are represented by the ends of the black arrows in Figure 5. For the observational cluster masses, we use the following values: $1.58 \times 10^5 M_\odot$ for NGC 330 (L. R. Patrick et al. 2020), $2.3 \times 10^4 M_\odot$ for NGC 2004 (D. E. McLaughlin & R. P. van der Marel 2005; F. Niederhofer et al. 2015), $1.5 \times 10^5 M_\odot$ for NGC 2100 (L. R. Patrick et al. 2016), and $2.57 \times 10^4 M_\odot$ for NGC 1818 (D. E. McLaughlin & R. P. van der Marel 2005; A. P. Milone et al. 2018). We remind readers that the scaled results are influenced by uncertainties in the estimated cluster masses, which themselves are highly uncertain. For instance, L. R. Patrick et al. (2016) provided an upper limit on the dynamical mass of NGC 2100, which is 6 times larger than the photometric mass reported in D. E. McLaughlin & R. P. van der Marel (2005). Where available, for consistency, we adopt dynamical masses for the clusters, which avoids assuming a mass-to-light ratio to determine the total mass of the cluster. Despite the sensitivity of the predicted number of RSGs to various factors (see Section 4.4), our predictions align reasonably well with the observed numbers.

However, it is important to note that the actual number of RSGs originating from noninteraction binaries, ZAMS mergers, and stable mass transfer could differ significantly from our simulation predictions. As explained in Section 2.2, the fractions of noninteraction binaries and ZAMS/pre-MS mergers in young open clusters are highly uncertain. Nevertheless, the evolution of stars in these two populations is identical to that of single stars. Consequently, the uncertainty in these populations can be effectively modeled by varying the assumed binary fraction in star clusters (see Appendix F).

The actual number of RSGs originating from stable mass transfer in young star clusters should be lower than shown in Figure 5, once the effects of SN kicks and reverse mass transfer are considered. In Appendix G, we demonstrate that SN kicks significantly affect stars in clusters aged approximately 15–50 Myr. For binaries where the primary star undergoes an SN explosion, over 90% are disrupted due to SN kicks (see also C. Wang et al. 2024). The typical velocity imparted to the secondary star is on the order of tens of $\mathrm{km\,s^{-1}}$, which may exceed the typical escape velocity (approximately 12–15 $\mathrm{km\,s^{-1}}$) of young open clusters (S. F. Portegies Zwart et al. 2010; P. Goudfrooij et al. 2014). Consequently, the majority of these disrupted binaries are expected to produce runaway RSGs. However, there are currently no examples of RSG runaway stars identified in the MCs. Examining the cluster population of NGC 330 as an example, between one and five RSGs could be considered candidate runaway stars based on their projected separation from the cluster center (see the distinction between the cluster and field populations in W. Narloch et al. 2021). However, their Gaia DR3 proper motions do not clearly corroborate this. Binaries that either do

Table 1
Summary of Properties of RSGs Originating from Various Evolutionary Scenarios, as Predicted by Our Single and Binary Models

Pathway	Produce RSGs or BSGs?	RSG Luminosity Extension	Remain in Clusters?
Single-star evolution	Can be both	∼0.14 dex	Yes
Pre/noninteraction binaries	Can be both	∼0.14 dex	Yes
Pre-MS/ZAMS mergers	Can be both	∼0.14 dex	Yes
MS mergers	Can be both	Up to ∼1 dex	Yes
Post-MS mergers	Most likely BSGs, hard to produce RSGs	Likely resembles single-star evolution	Yes
Case B mass transfer	Most likely runaway RSGs or blue stripped stars	∼0.18 dex	Mostly no
Case A mass transfer	BSGs or blue stripped stars, unlikely to produce RSGs	Cannot exceed that of MS mergers	⋯

not experience SN explosions, i.e., those that form black holes (BHs) or white dwarfs (WDs), or remain bound after the SN event are likely to undergo reverse mass transfer from the secondary star to the compact object, resulting in tripped helium stars before they reach the RSG phase. Accounting for these two effects, we find that, on average, 80%–90% of the RSGs predicted in our standard simulations may not persist as RSGs in young open clusters aged between 20 and 50 Myr (see Figure G1).

A more helpful comparison is examining the fraction of red stragglers, which are likely predominantly formed through MS mergers. The brown dashed line in Figure 5 shows that the fraction of RSGs originating from MS mergers relative to those from all the considered scenarios remains below approximately 12% across different ages, which is significantly lower than the observed value of approximately 63%–88% when identifying RSGs with $\Delta \log L \geqslant 0.2$ as red stragglers.

4. Discussions

4.1. Red Straggler Fraction

We summarize the properties of RSGs evolving from different scenarios and their properties in Table 1. Our simulations suggest that MS mergers are likely the primary contributors to the population of red stragglers in star clusters. Figure 5 shows that our standard simulations predict approximately 90% of RSGs to have luminosities consistent with single-star evolution (with a spread of approximately 0.14 dex), while the remaining 10% are predicted to have higher luminosities, contributing to the red straggler population. However, observations reveal that a much larger fraction of RSGs (63%–88%) have luminosities at least 0.2 dex higher than the least luminous RSGs in young young open clusters. Excluding RSGs originating from noninteraction binaries, ZAMS mergers, and stable mass transfer can increase the predicted red straggler fraction to 20%–40% between 20 and 50 Myr. Nonetheless, it is unlikely that all these populations are absent, particularly given that the ZAMS/pre-MS merger fraction is expected to be higher than our simulations suggest (C. Wang et al. 2022). Additionally, this upper limit of 40% is achieved at 20 Myr, a point at which we already underpredict the total number of RSGs observed in NGC 2004. Therefore, further removing populations from our standard simulations is not anticipated. Assuming a power-law initial orbital period distribution skewed toward short periods with $f(\log P) \propto \log P^{\pi}$ with $\pi = -0.55$ (H. Sana et al. 2012) could further increase the fraction of MS mergers (i.e., red stragglers) by a factor of about 2.

Moreover, triple-star evolution has been proposed as a mechanism that can trigger mergers of inner binaries through the von Zeipel–Lidov–Kozai cycles (H. von Zeipel 1910;

Y. Kozai 1962; M. L. Lidov 1962), which could also increase the red straggler fraction. However, the fraction of triple systems and their contributions in star clusters remain poorly understood. Interestingly, L. R. Patrick et al. (2024) found that in a significant fraction (5 out of 16) of binaries consisting of an RSG and an MS B-type star, the RSG appears significantly younger than its MS companion. Such systems can be explained by triple-star evolution, where the inner binary merges to form a red straggler that appears younger than its MS companion.

From the observational side, in NGC 2004, NGC 2100, and NGC 330, there seems to be a boundary at $\Delta \log L = 0.4$, above and below which the observed RSGs are grouped. Stars above this boundary are likely red stragglers originating from binary mergers. Using this threshold to identify red stragglers results in red straggler fractions of 23%–42% in these three clusters, which aligns with our discussions above. RSGs with luminosities below this threshold are likely the result of scenarios resembling single-star evolution. However, single-star evolution alone can account for only a luminosity extension of approximately 0.14 dex. To explain these intermediate-luminosity RSGs, an additional luminosity extension of approximately 0.26 dex from nonbinary effects is required.

4.2. Explanations for Intermediate-luminous RSGs

4.2.1. Observational Uncertainties

The observational uncertainty of 0.2 dex (±0.1 dex) used in this Letter is derived by comparing luminosities determined from SED fitting with the technique of B. Davies et al. (2013; see, for example, the comparison in L. R. Patrick et al. 2024). This value is smaller than the uncertainty of approximately 0.34 dex (±0.17 dex) obtained using the K-band magnitude or luminosity calibration presented in B. Davies et al. (2013). However, it may still represent an overestimate (L. Patrick 2024, private communication).

Studies have shown that variability is common among RSGs, which can influence the accuracy of their luminosity measurements. In the V band, variability can reach up to 4 mag, equivalent to 1.6 dex in luminosity (L. L. Kiss et al. 2006; E. Guinan et al. 2020). This large variability is because that the spectral appearance of RSGs in the visual bands is dominated by large TiO molecular features, which are well documented to be significantly variable. In contrast, variability in the near-infrared bands is believed to be substantially smaller (M. D. Soraisam et al. 2018; M. Yang et al. 2018). A typical variability of 0.08 mag is observed in the K band (from which the RSG luminosities used in this study are derived), with extreme cases reaching up to 0.25 mag (P. R. Wood et al. 1983; P. Massey et al. 2009). The extreme amplitude of this 0.25 mag

corresponds to a change in luminosity of 0.1 dex, which is well within the uncertainties on the luminosities. However, studies on the variability of RSGs in the near-infrared are still rare. Further studies are crucial for understanding how this variability contributes to the luminosity spread of RSGs in young open clusters.

4.2.2. Rotational Mixing

Rotational mixing is proposed to be an important mechanism to drive stellar rejuvenation (see A. Maeder & G. Meynet 2000 for a review). In our models, rotational mixing is inefficient, such that the MS lifetime of moderately rotating stars differs only slightly (by less than a few percent) from that of nonrotating stars. In contrast, in models with efficient mixing, such as the Geneva models (S. Ekström et al. 2012), the MS lifetime can be extended by up to about 25%. This implies that fast-rotating stars ignite helium later than their nonrotating counterparts and may have higher luminosities during their RSG phase. In Appendix H, we explore the effects of stellar rotation by analyzing Geneva models. We find that while efficient rotational mixing can lead to enhanced rejuvenation and longer MS lifetimes, fast-rotating stars generally remain blue during their helium-burning phases and are thus unlikely to contribute significantly to the RSG population. It is worth noting that in Geneva models with masses above $10\,M_\odot$, even nonrotating stars remain mostly blue. Whether a star manifests as a BSG or an RSG is highly sensitive to internal mixing processes, which remain poorly constrained. Future theoretical studies, particularly on the combined effects of various internal mixing processes, are essential for a comprehensive understanding of the role rotational mixing plays in the luminosity spread of RSGs in young open clusters.

4.2.3. Real Age Difference

Real age difference can also cause a luminosity extension of RSGs in young open clusters. It is important to note that unlike old and massive globular clusters, which show evidence of multiple stellar generations (R. G. Gratton et al. 2012; N. Bastian & C. Lardo 2018), current studies of young open clusters argue against significant real age differences among their stars (see Appendix I for detail). However, small age differences may exist in young open clusters (less than approximately 5 Myr; see Figure I1). C. Wang et al. (2022) proposed that approximately 10%–30% of binaries may merge due to orbit decay within the first ∼2 Myr after their formation. Such early mergers experience rejuvenation, making them appear up to 2 Myr younger than other stars. While this is not a true age difference, it effectively mimics one because it occurs early in the cluster evolution, and the fraction of such early mergers is high. In Figure I2, we illustrate that a real age difference of 2 Myr can lead to a luminosity extension ranging from 0.03 to 0.07 dex within the age range of the observed clusters. A real age difference of 5 Myr can result in a significantly larger luminosity extension, spanning from 0.1 to 0.18 dex within the same age range. When combined with contributions from single-star evolution (∼0.14 dex) and observational uncertainties (0.2 dex), the total luminosity extension amounts to approximately 0.4–0.5 dex. This is sufficient to explain the observed population of low-to-intermediate-luminosity RSGs in young open clusters.

4.2.4. Measurement Accuracy of the Least Luminous RSG

The luminosity extension of the observed RSGs is determined by the least luminous RSG in these clusters. In NGC 2004, NGC 2100, and NGC 1818, the two to three least luminous RSGs are noticeably less luminous than the luminosity where a significant fraction of RSGs accumulate ($\Delta \log L$ ranges from 0.25 to 0.4 in NGC 2004 and NGC 2100 and from 0.5 to 0.6 for NGC 1818). Excluding these outliers would significantly improve the agreement between predictions and observations. Therefore, future studies to confirm whether these two to three least luminous RSGs are genuine cluster members and to accurately measure their luminosities are crucial.

In summary, we argue that the observed low-to-intermediate-luminosity RSGs (with extensions up to approximately 0.4–0.5 dex) are likely the result of processes resembling single-star evolution. In contrast, RSGs with higher luminosities are more likely red stragglers originating from MS mergers. It is important to note that the uncertainties mentioned above also apply to the interpretation of red stragglers, as our simulations predict their luminosity peak at $\Delta \log L$ between 0.2 and 0.4.

4.3. RSGs as Indicators of Cluster Age

Estimating the age of young open clusters is a critical yet challenging task, particularly due to the presence of an extended MS turnoff, which complicates the traditional approach of using the MS turnoff as an age indicator. E. R. Beasor et al. (2019) and N. Britavskiy et al. (2019) proposed that the least luminous RSG in a cluster serves as a reliable age indicator, as it likely represents the oldest RSG in the cluster and is expected to be a product of single-star evolution. J. J. Eldridge et al. (2020) examined BPASS single and binary models and suggested that the mean luminosity of the entire RSG population is a better age indicator. They argued that while binary evolution can produce a larger luminosity spread among RSGs, the mean luminosities derived from single and binary scenarios remain nearly identical. Consequently, they advocated for using the entire RSG population rather than just the least luminous RSG.

We disagree with the conclusion of J. J. Eldridge et al. (2020), as our simulations indicate that the high-luminosity RSG population is predominantly composed of binary merger products. J. J. Eldridge et al. (2020) examined the luminosity ranges produced by single and binary evolution but did not account for the relative time a star spends at each luminosity. Our population synthesis simulations based on detailed binary models demonstrate that MS mergers are the primary contributors to the luminosity spread of RSGs.

To determine cluster age, it is essential to focus on RSGs originating from scenarios resembling single-star evolution. Stellar evolutionary models predict a small luminosity spread of approximately 0.14 dex for these scenarios. However, when comparing these predictions with observed distributions of RSGs, we argue that an additional luminosity extension, potentially caused by observational errors and real age differences, must be considered. As explained in Section 4.2, low-to-intermediate-luminosity RSGs (with extensions up to approximately 0.4–0.5 dex) are likely the result of processes consistent with single-star evolution. Therefore, we propose that the mean luminosity of this population serves as a more reliable indicator of cluster age.

4.4. The Impact of Uncertain Physics

4.4.1. Single-star Evolution

The evolution of massive stars into RSGs and the duration of this phase are sensitive to stellar internal mixing and wind mass loss during the RSG phase, both of which are still not well understood (S.-C. Yoon & M. Cantiello 2010; N. Smith 2014; A. Schootemeijer et al. 2019; E. Zapartas et al. 2024).

In this work, we adopt efficient semiconvective mixing with $\alpha_{SC} = 10$. A. Schootemeijer et al. (2019) show that for $\alpha_{SC} \geqslant 1$, the evolutionary outcomes remain similar. We use a mass-dependent overshooting parameter that ranges from 0 to 0.33. As shown in Figure A1, our SMC models with masses between 5 and $16.6\,M_\odot$ evolve into RSGs and subsequently undergo a blue loop. Star models above $19\,M_\odot$ ignite helium as BSGs, with only some evolving to the red side during the helium-burning stage. For the LMC models, stars with masses below approximately $15\,M_\odot$ do not experience a blue loop. Varying these internal mixing parameters can influence the occurrence of a blue loop (A. Schootemeijer et al. 2019). While this uncertainty can affect the predicted number of RSGs, it does not influence the luminosity of RSGs. Therefore, our conclusion that red stragglers may result from MS mergers remains unaffected.

Mass loss of RSGs also remains poorly constrained, particularly at low metallicities. This uncertainty does not significantly influence the luminosity of RSGs, but it has a substantial impact on their lifetimes. Consequently, the predicted luminosity extension of RSGs is unaffected by this uncertainty, but the predicted number of RSGs can vary. E. Zapartas et al. (2024) explored the impact of varying mass-loss rates on the formation and evolution of RSGs in the SMC. They found that higher mass-loss rates, such as those in N. D. Kee et al. (2021) and M. Yang et al. (2023), lead to earlier envelope stripping and shorter RSG lifetimes. In contrast, lower mass-loss rates, such as those in E. R. Beasor et al. (2020), can extend the RSG phase. M. Yang et al. (2023) derived an empirical mass-loss prescription for RSGs based on a large sample of stars in the SMC, which is slightly higher than the rates used in our models. Adopting this empirical prescription would likely reduce the predicted number of RSGs.

In summary, the predicted luminosity spread of RSGs, a key factor in constraining their origins, remains unaffected by uncertainties in single-star evolution. However, the total number of RSGs is sensitive to these uncertainties. Further comprehensive studies on comparing the observed and predicted ratio of RSGs to BSGs/YSGs in young open clusters may offer valuable constraints on uncertain mixing processes and mass-loss prescriptions.

4.4.2. Mass Transfer Stability and Efficiency

Mass transfer stability and efficiency remain the least understood aspects of binary evolution. Previous studies (B. Hastings et al. 2021; C. Wang et al. 2022) have pointed out that to explain the high number of Be X-ray binaries in the SMC (F. Haberl & R. Sturm 2016) and the large fraction of Be stars in young open clusters (A. P. Milone et al. 2018), a greater fraction of binaries must undergo stable mass transfer than is currently predicted by our models. In addition, a higher mass transfer efficiency than predicted by our models has also been suggested as essential for explaining the observed properties of

Be X-ray binaries (Y. Shao & X.-D. Li 2014; S. Vinciguerra et al. 2020; K. A. Rocha et al. 2024).

However, whether a higher mass transfer efficiency contributes to the population of red stragglers remains uncertain. On the one hand, whether the rejuvenated star evolves to an RSG or a BSG depends on the efficiency of internal mixing processes. If the rejuvenation is complete, the star's subsequent evolution would resemble that of a single star and may evolve into an RSG (this statement may apply to all processes capable of inducing rejuvenation, including stellar rotation). However, incomplete rejuvenation might result in the star evolving into a BSG rather than an RSG. On the other hand, as previously mentioned, after considering the effects of SN kicks and reverse mass transfer, the stable mass transfer scenario is not expected to significantly contribute to the RSG population in clusters younger than about 50 Myr.

4.4.3. Post-MS Mergers

In our simulations, we do not track the evolution of the mergers involving a post-MS star due to the lack of well-studied, detailed models. These mergers typically have a helium core from the post-MS star and an envelope that mixes the post-MS star's envelope with the entire MS star. Therefore, such merger products have a lower core-to-envelope mass ratio compared to single stars of equivalent total mass. Previous studies using simplified models suggest that these merger products are likely to ignite helium as BSG or YSG stars and may remain in these phases without evolving into RSGs (H. Braun & N. Langer 1995; S. Justham et al. 2014; E. P. Bellinger et al. 2024; F. R. N. Schneider et al. 2024).

Excluding post-MS mergers from our analysis does not impact our predictions regarding the maximum luminosity of red stragglers in young open clusters for several reasons. First, in a cluster, the mass of RSGs from post-MS mergers cannot exceed that of mergers between two MS turnoff stars, as they experience stronger rejuvenation. Second, although the initial luminosity of post-MS merger products depends on their total mass, their luminosity is expected to decrease as they evolve toward the RSG phase, where luminosity is primarily determined by core mass (F. R. N. Schneider et al. 2024). Post-MS mergers generally have smaller core masses than MS mergers due to weaker rejuvenation. Finally, S. Justham et al. (2014) suggested that merger products with a lower core-to-envelope ratio remain blue for longer, meaning that more massive post-MS mergers from higher-mass-ratio binaries, which could produce more luminous RSGs, are less likely to evolve into RSGs at all. In summary, excluding post-MS mergers does not affect the predicted luminosity range of RSGs formed through binary evolution, nor does it alter our conclusion that MS mergers are responsible for the most luminous RSGs in young open clusters.

However, excluding post-MS mergers may impact the predicted number of RSGs. F. R. N. Schneider et al. (2024) show that post-MS mergers can evolve redward, depending on the mass the primary star accreted and the detailed structure of the merger envelope. It is important to note that a significant number of our models (around 50%, depending on stellar masses) merge in the post-MS phase (see Figure B1). However, as previously mentioned, if these mergers do evolve into RSGs, they may contribute to low-to-intermediate-luminosity RSGs. To accurately assess the impact of post-MS mergers on the population of RSGs in young open clusters, it is crucial to

develop detailed models for these mergers. Additionally, a better understanding of the stability of binary mass transfer is needed.

5. Concluding Remarks

The observed luminosity extension of RSGs in young open clusters presents a clear challenge to the single-star origin scenario. In this Letter, we present a comprehensive analysis of the luminosity of RSGs in young open clusters (with ages up to 100 Myr) using state-of-the-art detailed binary-evolution models that incorporate empirical initial binary parameter distributions. These models have previously been employed to successfully explain the observed multiple components of MS stars in young open clusters.

Our findings reveal that single-star evolution and processes resembling single-star evolution, including pre/noninteraction binaries and pre-MS or ZAMS mergers, typically produce RSGs that occupy the lowest luminosity range, spanning approximately 0.14 dex in $\log L$. In contrast, MS mergers result in a significantly broader luminosity spread of up to a factor of 10 (1.0 dex in $\log L$). This luminosity extension remains robust despite uncertainties in the physics of both single- and binary-star evolution. This predicted luminosity extension aligns well with the observed spread of RSG luminosities in young open clusters, suggesting that the observed high-luminosity red stragglers are strong candidates for being products of MS mergers.

However, our predictions indicate an overabundance of low-luminosity RSGs from scenarios resembling single-star evolution, which does not match observations. To reconcile this discrepancy, we find that factors such as observational accuracy, RSG variability, and a small age spread of less than approximately 5 Myr are necessary. These uncertainties, combined with the intrinsic luminosity spread caused by single-star evolution, can produce a total luminosity spread of up to a factor of 3 (0.5 dex), offering a much better explanation for the observed luminosity distributions of RSGs. Nevertheless, fully addressing this discrepancy will require future studies on accurately measuring the luminosities and variabilities of RSGs in a larger sample of young open clusters, with particular attention to the low-luminosity population.

Our findings suggest that, instead of relying on the previously proposed least luminous RSG or the average luminosity of the entire RSG population to determine cluster age, the average luminosity of the low-to-intermediate-luminosity RSG population (up to a factor of approximately 3) serves as a more reliable indicator of cluster age.

Our study offers valuable insights into the formation of RSGs with varying luminosities in young open clusters, paving the way for future observational campaigns. The higher-luminosity RSGs offer a unique opportunity to explore the physics and frequency of binary mergers, whereas detailed investigations of the lower-luminosity population are essential for advancing our understanding of diverse evolutionary pathways, including single-star evolution, stable mass transfer, and post-MS mergers.

Appendix A
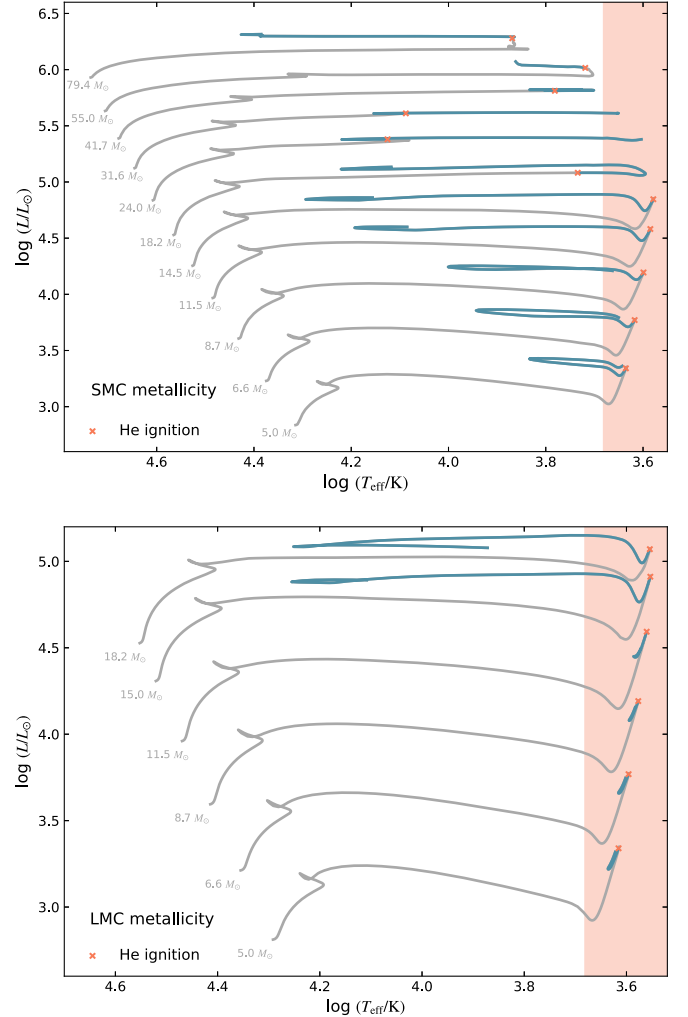## Single-star Evolution and Comparison with Observations

In Figure A1, we present the evolution of our SMC and LMC single-star models in the HRD, with central helium ignition and helium-burning phases highlighted. The appearance of a blue loop is shown to be sensitive to metallicity. SMC models below approximately 18 $M_\odot$ ignite helium as RSGs and

Figure A1. Evolution of our nonrotating single-star models with SMC metallicity (upper) and LMC metallicity (lower) in the HRD. Gray lines indicate the pre-helium-ignition phase, while blue lines represent the central helium-burning phase. Orange crosses mark the positions where central helium ignition occurs. The reddish shaded area indicates the region where stars are classified as RSGs in this study.
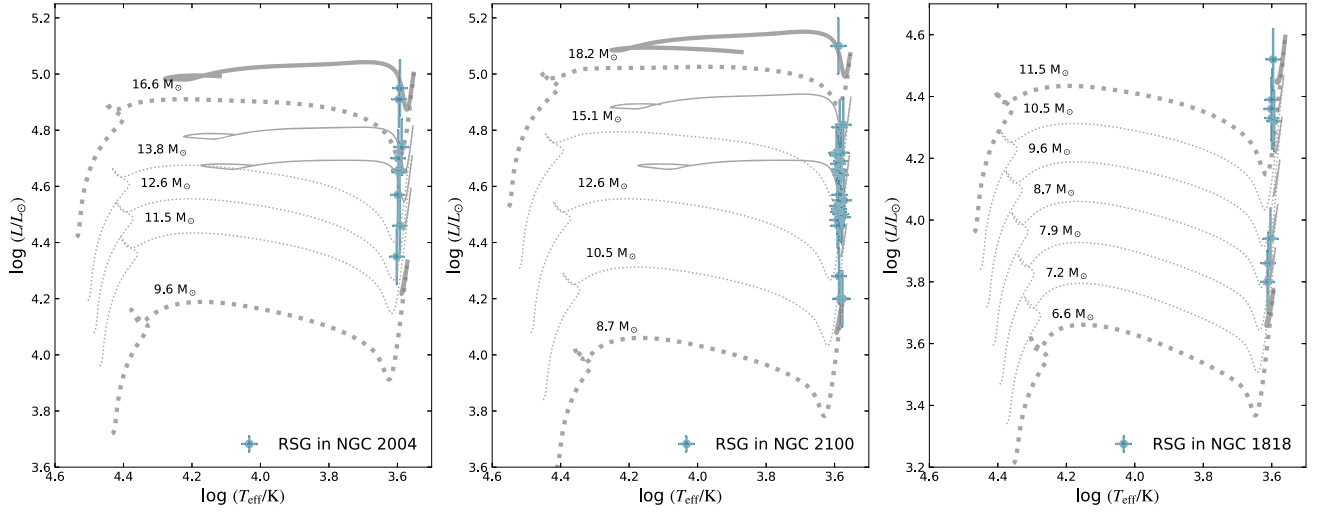
Figure A2. Same as Figure 1 but for the comparison of observed RSGs in three LMC clusters, NGC 2004, NGC 2100, and NGC 1818 (E. R. Beasor & B. Davies 2016; E. R. Beasor et al. 2019; N. Britavskiy 2024, private communication), with our LMC single-star models.

subsequently undergo a blue loop excursion. In contrast, for LMC models, only stars more massive than about $15\,M_\odot$ exhibit a blue loop. For SMC models above $18\,M_\odot$, stars ignite helium at higher temperatures and may or may not become RSGs.

In Figures A2, we compare LMC single-star models with RSGs detected in three young LMC clusters. The same conclusion is achieved that the luminosity ranges of the observed RSGs in these clusters are too large to be explained by single-star evolution. The apparent ages of the least and most luminous RSGs derived from these single-star tracks are 25 and 13 Myr for NGC 2004, 30 and 11 Myr for NGC 2100, and 48 and 21 Myr for NGC 1818, respectively. Here we utilize nonrotating star models. As discussed in C. Wang et al. (2023), stellar rotation does not significantly affect the evolution of stars in our models unless they initially rotate at exceptionally high velocities (larger than approximately 70% of their breakup velocities) due to the assumption of inefficient rotational mixing.
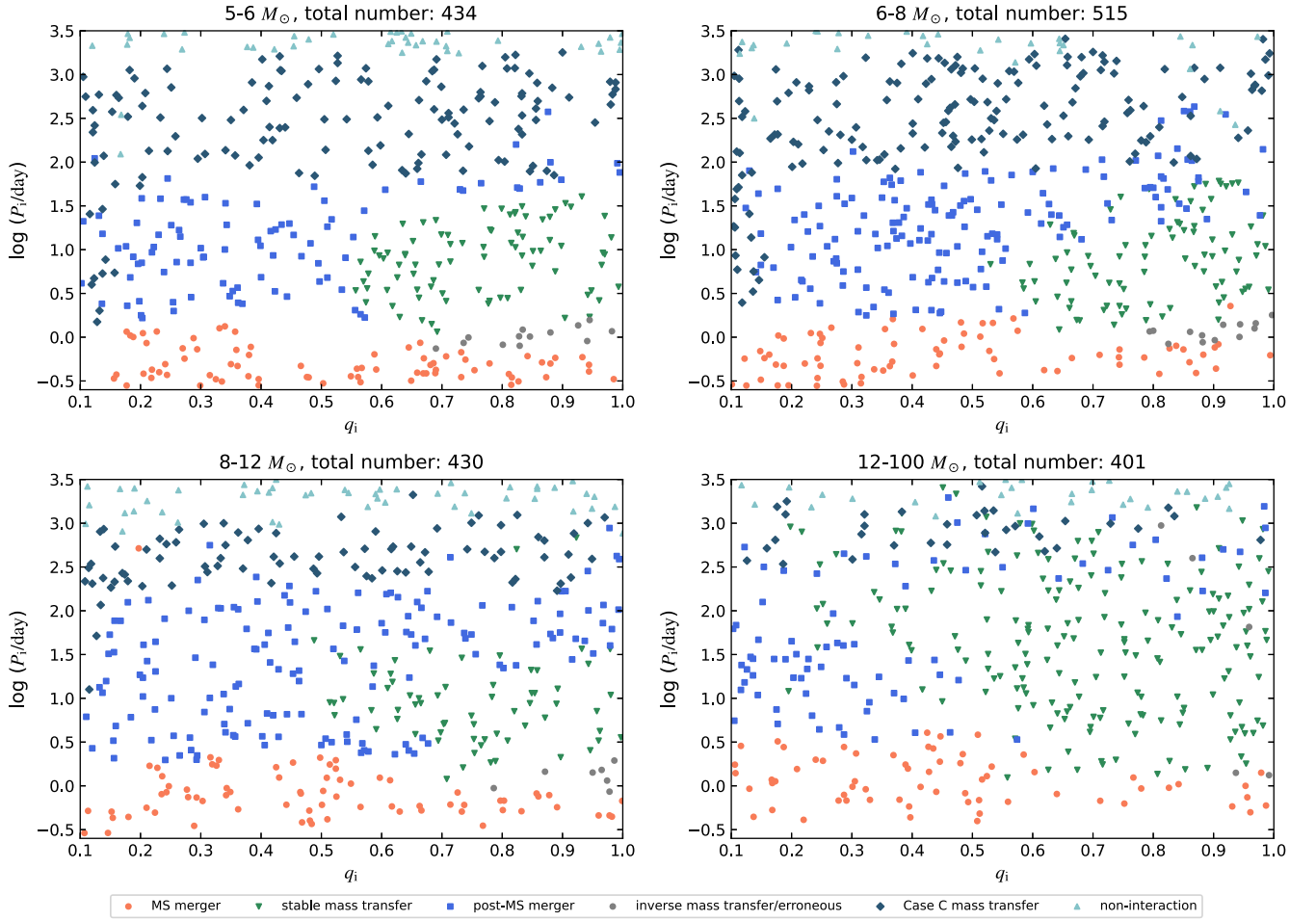
Our single-star models terminate at the end of central helium exhaustion. Here we also examine post-helium-burning evolution using our noninteracting binary models, which are followed until the end of carbon depletion. In Figure A3, we present the luminosity evolution of these models alongside the lifetime ratio of AGB stars to helium-burning stars. The result show that after helium exhaustion, stars experience a rapid increase in luminosity. Consequently, the contamination of AGB stars within the helium-burning star population remains low, with approximately 4% in 20 Myr clusters and up to ~20% in 100 Myr clusters. Notably, the fraction of significantly more luminous AGB stars, those exceeding their helium-burning counterparts by 0.5 dex (or 1 dex), is consistently below 2% (or 0.3%). These findings suggest that while AGB stars may account for the observed low-luminosity population of RSGs, they are insufficient to explain the high-luminosity population observed in young open clusters.

In this section, we also present the luminosity extension $\Delta \log L$ of RSGs that evolved from pre/noninteraction binaries that resemble single-star evolution in Figure A4. The rare cases of $\Delta \log L \gtrsim 0.1$ are due to contamination from AGB stars,
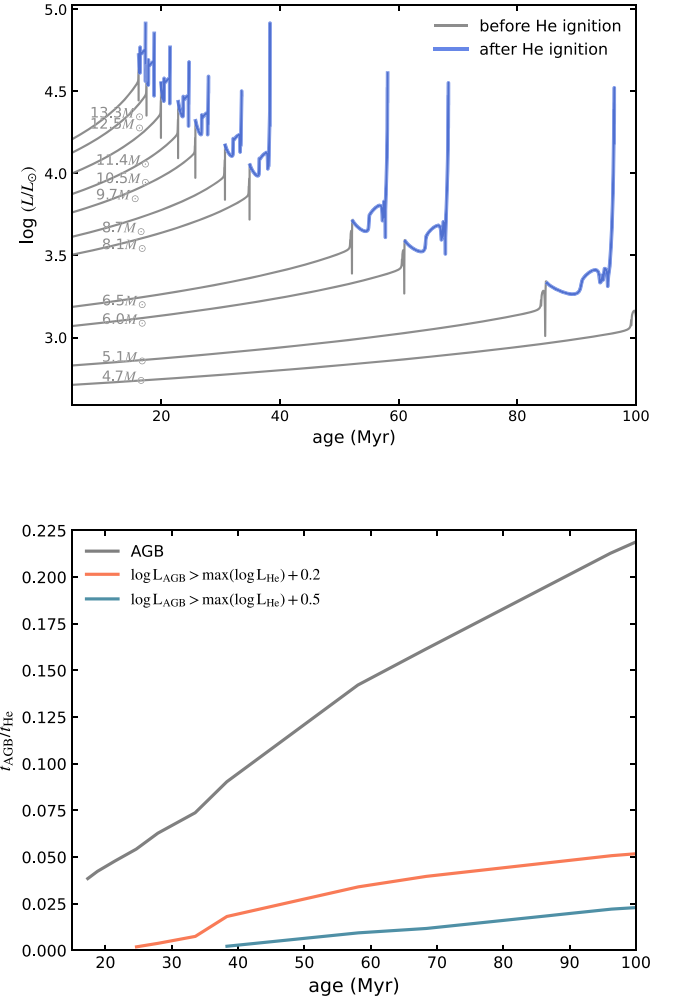
Figure A3. Upper: luminosity evolution of exemplary models in our noninteracting binaries, shown before (gray lines) and after (blue lines) central helium exhaustion. Lower: the ratio of the AGB star lifetime to that of their helium-burning counterparts. The gray line represents the entire AGB phase, while the orange and blue lines correspond to AGB stars with luminosities exceeding the maximum luminosity during their helium-burning phase by 0.2 dex and 0.5 dex, respectively.

Figure A4. Same as Figure 4 but for RSGs originating from binaries that have not undergone mass transfer or will never do so.

whereas the rare cases of $\Delta \log L \lesssim -0.06$ are due to contamination from pre-helium-burning red stars.

Appendix B
Binary Evolutionary Examples

In Figure B1, we display the evolutionary outcomes of our detailed binary models. We focus on binaries with primary masses above $5\,M_\odot$, as we only consider clusters up to 100 Myr. For binaries experiencing inverse mass transfer or encountering numerical errors, we stop the calculations as soon as these events occur. Such cases constitute a small fraction (around 2%) of the models. Inverse mass transfer binaries typically start with high mass ratios, allowing the secondary star's mass to exceed that of the primary during the first mass transfer phase. In these systems, the secondary star completes hydrogen burning first and subsequently transfers material to the primary. Due to extreme mass ratios, these binaries are expected to merge, and similar to normal Case B mergers, they may primarily produce BSGs/YSGs.

For binaries undergoing Case C mass transfer, we stop calculations once the mass transfer rate reaches the ad hoc threshold of $10^{-1}\,M_\odot\,\mathrm{yr}^{-1}$ and assume that these systems will merge. Our simulations include the contributions to the RSG population from primary stars prior to the onset of Case C mass transfer. We disregard the possibility that the secondary star could survive common envelope evolution and later become an RSG. This assumption is reasonable, as even if the envelope is successfully ejected, the post-common-envelope orbital separation would likely be too small to permit RSG formation. Instead, the secondary would transfer material to the remnant of the primary before evolving into an RSG.

Figure B2 displays the evolution of two example binary models in the HRD, corresponding to Case A mass transfer and Case B mass transfer, respectively. For Case B mass transfer, despite the accretor reaching critical rotation after accretion, its subsequent evolution closely resembles that of a genuine single star with the same total mass. This is because rotationally induced mixing remains negligible due to the presence of a strong chemical gradient in the stellar interior. The upper panel shows that although the accretor in Case A mass transfer accretes more material, it does not contribute to the red straggler population, as it remains blue throughout the entire helium-burning phase.

Figure B1. Evolution outcomes of our detailed binary models. Each marker represents a binary model with the initial primary mass within the indicated mass range. The initial mass ratio (defined as the primary star's mass divided by the secondary star's mass) and orbital periods are shown on the x- and y-axis, respectively. The total number of binaries in each panel is also provided. We identify six distinct evolutionary outcomes for our binary models: MS mergers (orange circles), stable mass transfer (green upside-down triangles), post-MS mergers (blue squares), inverse mass transfer/errors (gray circles), Case C mass transfer (dark blue diamonds), and wide binaries that do not interact (light blue triangles). In our simulations, RSGs can originate from MS mergers, stable mass transfer, noninteraction binaries, and Case C binaries before mass transfer occurs.
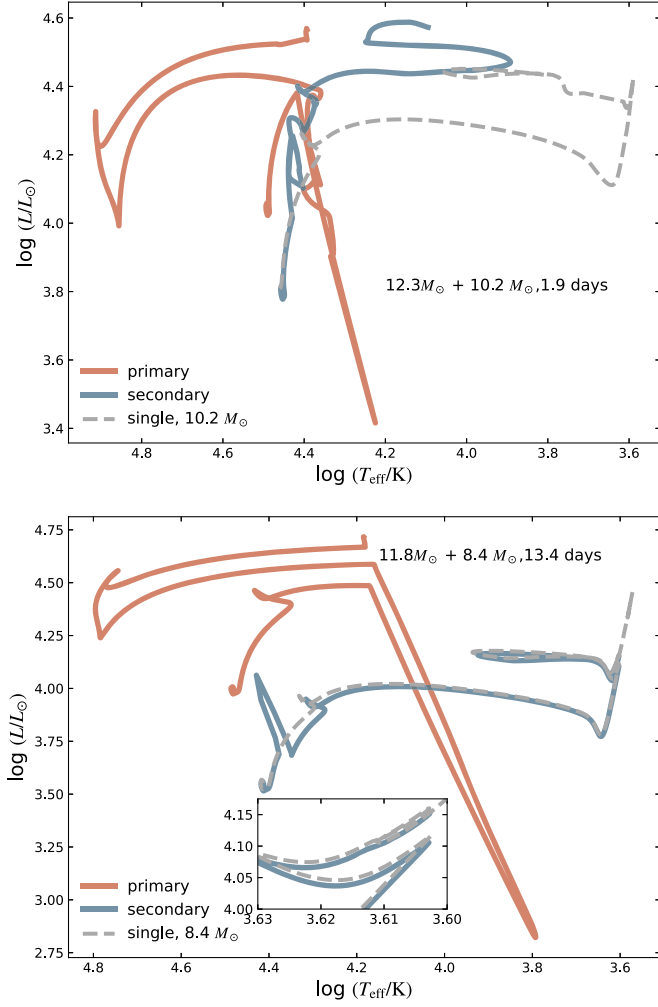
Figure B2. Evolution of both components of two binary systems (upper: Case A; lower: Case B) with initial parameters indicated. The orange and blue solid lines depict the evolutionary tracks of the primary and secondary star, respectively. The gray dashed line represents the evolution of a single-star model that has the same mass as the initial mass of the secondary star. The inset of the lower panel is a zoom-in of the tip of the supergiant phase.

Appendix C
Definition of Baseline Luminosity L_0

In this section, we describe how we define the baseline luminosity of RSGs (L_0), used to assess the luminosity spread of RSGs in young open clusters. In Figure C1, we show the luminosity evolution over time for our single-star models (see Figure A1). For each mass, we calculate the weighted mean logarithmic luminosity $\log L_0$ during the RSG phase (we ignore the second RSG phase after the blue loop if it exists, as its duration is much shorter than the first RSG phase) according to the following expression:

$$\log L_0 = \frac{\sum_{i=i_{\text{start}}}^{i=i_{\text{end}}} \log L_i * (t_{i+1} - t_i)}{\sum_{i=i_{\text{start}}}^{i=i_{\text{end}}} (t_{i+1} - t_i)},$$

where i_{start} and i_{end} are the indices for the start and end of the RSG phase in the MESA history file (i is the model number in the MESA history file) and $\log L_i$ and t_i denote the logarithmic
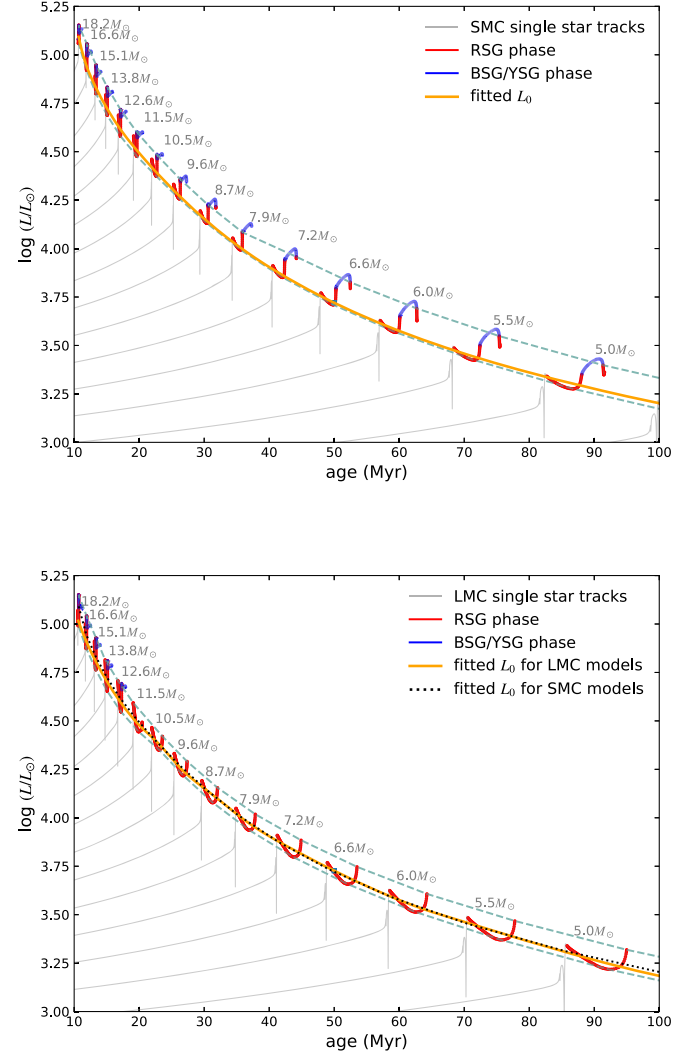
Figure C1. Luminosity–age diagram for our SMC (upper) and LMC (lower) single-star models. Thin gray lines show the evolution of stellar luminosity over time for models of various masses, as labeled. The red and blue lines denote the RSG phase and BSG/YSG phase, respectively. Turquoise dashed lines delineate the luminosity range during the helium-burning phase. The orange line represents the evolution of L_0 (see text) as a function of age. The black dotted line in the lower panel is the same as the orange line in the upper panel.

luminosity and age at index i. This approach accounts for the time the star spends at each luminosity. We define the mean age, age_0, of the RSG phase as $(t_{i_{\text{end}}} - t_{i_{\text{start}}})/2$. Then we get one data point (age_0, $\log L_0$) for each track in Figure C1. Using spline interpolation, we obtain the orange line in this figure, representing the evolution of $\log L_0$ over age. This figure shows that L_0 closely aligns with the helium ignition luminosity.

The choice of L_0 has minimal impact on our conclusions, as single stars exhibit only slight luminosity variation during the RSG phase. Comparing L_0 for LMC models (orange line in the lower panel of Figure C1) and SMC models (black dotted line in the lower panel of Figure C1), we find that metallicity has a negligible effect on L_0. This supports our comparison of detailed binary models with SMC metallicity to observed RSGs in LMC clusters (Figures 3 and 5).

Appendix D
Semianalytical Method for Estimating the Upper Limit for the RSGs from MS Merger Products

To address the problem of random sampling, we include a semianalytical analysis that establishes an upper limit for the luminosity extension due to MS mergers. We hypothesize that the most massive MS star in a cluster likely results from the merger of two turnoff-mass stars. Equal-mass mergers exhibit the strongest rejuvenation effects. These stars are expected to evolve into the most massive RSGs at a slightly later time. We use our single-star models with an initial rotational rate of 55% of the critical values for merger progenitors and single-star models with a rotational rate of 15% of the critical values for the merger products.

For a given age t_{merge}, we first calculate the terminal-age MS (TAMS) mass corresponding to this age and assume that two stars of this mass merge at this age. Using the method described in F. R. N. Schneider et al. (2016), we compute the mass of the merger product, m_{merger}, and its apparent age, t_{app}. Next, through interpolation, we identify the single-star model with an initial mass of m_{merger} and determine its maximum luminosity, L_{max}, as well as the age, t_{max}, at which this maximum luminosity is reached during the RSG phase. The actual age at which the rejuvenated merger product reaches its maximum luminosity is then given by $t = t_{\mathrm{max}} - t_{\mathrm{app}} + t_{\mathrm{merge}}$. By varying t_{merge}, we derive the relationship between t and L_{max}, which is represented by the thick solid gray curve in panel (a) of Figure 3.

This calculation accounts for mass loss during the merger process, which is typically less than 10% of the total mass of the merger progenitor (E. Glebbeek et al. 2013). If no mass loss is assumed during the merger process, $\Delta \log L$ would increase by approximately 0.1 dex.

Appendix E
Cumulative Luminosity Distribution for the RSGs Observed in Four Clusters

In Figure E1, we present the cumulative luminosity distribution of RSGs in four young open clusters. Using a threshold of $\Delta \log L$ between 0.4 and 0.5 to identify red stragglers, we find red straggler fractions of 22% in NGC 2004, 13%–42% in NGC 2100, 25%–30% in NGC 330, and 38%–63% in NGC 1818.
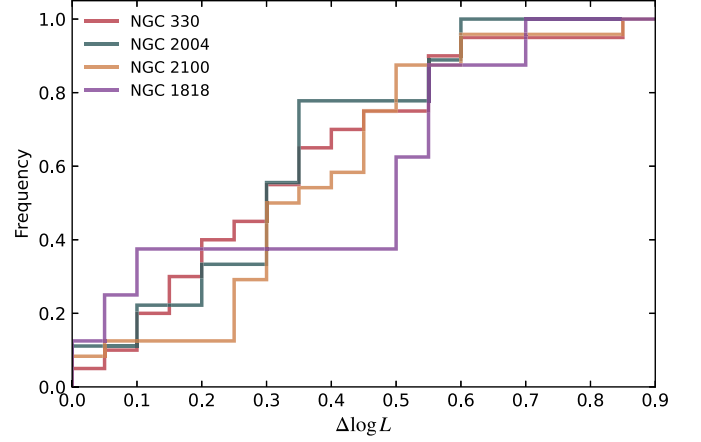

Figure E1. Cumulative distribution of $\Delta \log L$ for RSGs in four young open star clusters, as indicated in the legend. For each cluster, $\Delta \log L$ represents the luminosity difference, in logarithmic space, between each RSG and the least luminous RSG in that cluster.

Appendix F
Impact of Initial Binary Fraction

The results and conclusions in our main text are based on the extreme assumption of a binary fraction of 1. To explore the impact of varying initial binary fractions, we conduct a population synthesis simulation using only single-star models. Through a Monte Carlo approach, we generated an initial sample of 3670 single stars (matching the sample size in our binary-based simulation), with initial masses distributed according to the Salpeter IMF within 3 and $100\,M_\odot$ (the same mass range as primary stars in our binary models). We show the number of RSGs as a function of age predicted in this single-star simulation in the left panel of Figure F1. Compared to Figure 5, it can be seen that single-star evolution produces more RSGs, as a significant portion of our binary systems undergo post-MS mergers, which likely do not substantially contribute to the RSG population.

By combining this single-star simulation with our binary-star results, which represent an initial binary fraction of 50%, we calculated the fraction of RSGs originating from binary evolution (represented by the darkest blue bars in the right panel of Figure F1). We then increased the binary fraction to 60% and 70% by randomly selecting samples from the single-star simulation. The resulting contributions of binary evolution to RSG formation are shown with lighter blue bars in the right panel of Figure F1.
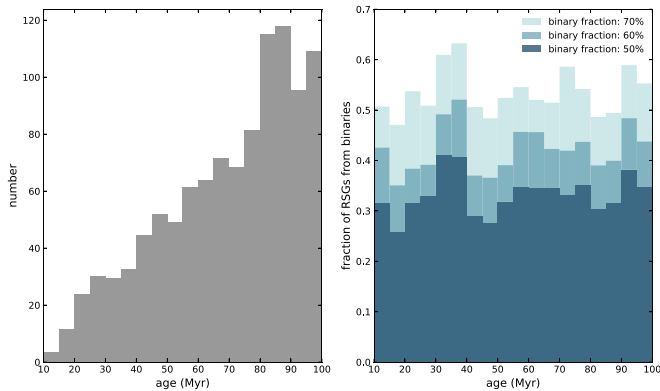

Figure F1. Left: predicted number of RSGs as a function of age from a population synthesis simulation based on 3670 single-star models with initial rotational velocities at 55% of their critical values. Right: fraction of RSGs originating from binary evolution, assuming different initial binary fractions as indicated.

Appendix G
Impact of SN Kicks and Reverse Mass Transfer

As described in the main text, our simulations assume that the secondary star evolves in isolation after the primary star forms a compact object. In this Appendix, we investigate the impact of SN kicks that may disrupt binaries and produce runaway RSGs. If a binary remains bound after the SN kick, the secondary star may initiate reverse mass transfer to the primary star before evolving into an RSG. Here we use the prescription in C. Wang et al. (2024) to determine the type of compact object formed by the primary star and the SN kicks imparted on them. Specifically, we assume zero kicks for BHs and a Maxwell–Boltzmann distribution with an rms velocity $\sigma = 265\,\mathrm{km\,s^{-1}}$ for neutron stars (NSs) formed through core-collapse SNe (G. Hobbs et al. 2005). For NSs formed from
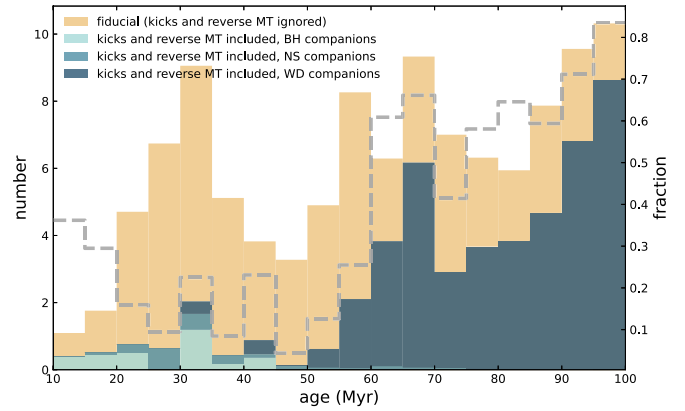
Figure G1. The impact of SN kicks and reverse mass transfer on the formation of RSGs in young open clusters originating from stable mass transfer. The yellow bars represent the predicted number of RSGs in clusters with an initial mass of $1.3 \times 10^5\,M_\odot$, originating from stable mass transfer in our simulations, as a function of age (the same as the yellow bars in Figure 5). The bluish bars show the predicted number of RSGs after accounting for the effects of SN kicks and reverse mass transfer, with light blue, medium blue, and dark blue corresponding to RSGs with BH, NS, and WD companions, respectively. The bluish bars are stacked. The fraction of these newly predicted RSGs relative to the values from our standard simulations is indicated by the gray dashed line and corresponds to the scale on the right y-axis.

electron-capture SNe, we assume smaller kicks from a flat distribution between 0 and $50\,\mathrm{km\,s^{-1}}$ (E. Pfahl et al. 2002; P. Podsiadlowski et al. 2004). For each binary system, we calculate the probability of the system remaining bound after the SN kicks and use this probability as a weight in our original predictions. For binaries that remain bound (including systems with BH or WD companions), we further compare the radius of the RSG formed by the secondary star to the orbital separation at the moment the primary forms a compact object (assuming the orbit remains unchanged thereafter). An RSG is allowed to form only if its radius is smaller than the orbital separation.

The results are shown in Figure G1. Before approximately 50 Myr, RSGs predominantly have BH or NS companions. For systems where the primary forms an NS, over 90% are disrupted by SN kicks. For systems where the primary forms a BH, a significant fraction will undergo reverse mass transfer unless the initial orbital period is large (greater than hundreds of days). After accounting for these effects, less than approximately 20% of the RSGs predicted by our original simulations are expected to remain in young open clusters between 20 and 50 Myr. After 50 Myr, the primary stars form WDs, and the impact of reverse mass transfer becomes much smaller compared to younger clusters.

Appendix H
Impact of Stellar Rotation

To better understand how rotation impacts the properties of RSGs in young open clusters, we examine Geneva models,[10] which employ more efficient rotationally induced mixing compared to our models (C. Georgy et al. 2013). Their evolutionary tracks in the HRD are shown in Figure H1. It is important to note that the Geneva models, formally labeled as having velocities at 95% of their critical angular velocities, do not actually rotate near the critical limit. As explained in C. Wang et al. (2023), due to the initial relaxation phase in the

---

[10] https://www.unige.ch/sciences/astro/evolution/en/database/syclist/
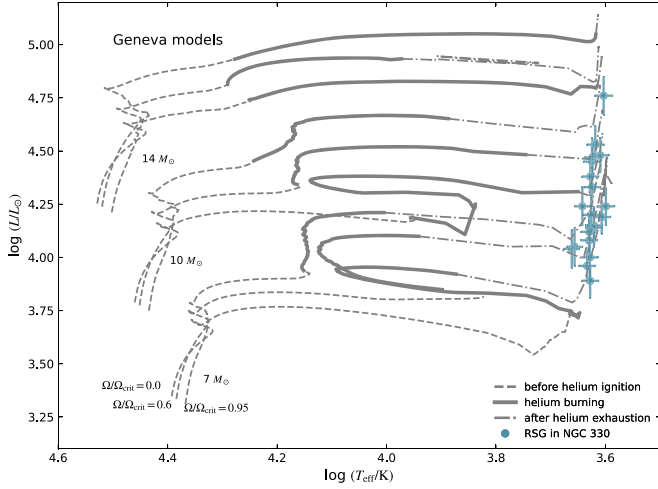
Figure H1. Evolution of Geneva single-star models with different initial rotation rates at SMC metallicity in the HRD. The masses are indicated in the figure. Dashed, solid, and dashed–dotted lines represent phases before central helium ignition, during helium burning, and after helium exhaustion, respectively. For each mass, three initial rotational velocities, 0%, 60%, and 95% of the critical angular velocity, are included. Observations of RSGs in NGC 330 are overplotted for comparison.
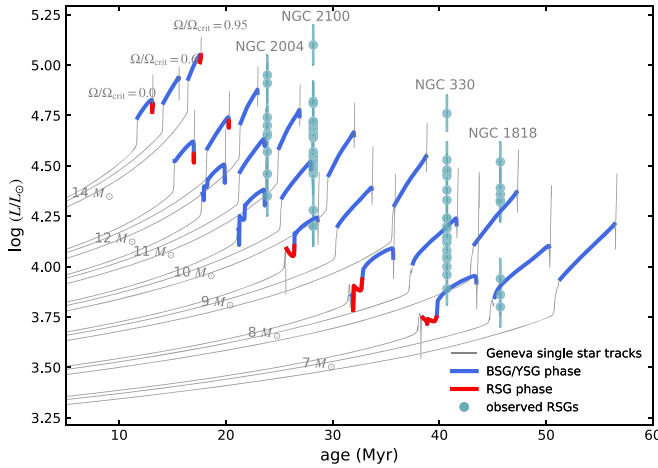
Figure H2. Luminosity vs. age for Geneva single-star models (thin gray lines) with corresponding masses indicated. For each mass, the three tracks represent initial rotational velocities of 0%, 60%, and 95% of the critical angular velocity, shown from left to right. The RSG and BSG/YSG phases are highlighted with thick red and blue lines, respectively. The observed RSGs in the four clusters analyzed in this study are shown as cyan dots with error bars.

Geneva models and differences in the definition of critical rotation, this velocity corresponds to only 55% of critical rotation in our single-star models.

In Figure H1, we see that while fast-rotating models experience significant rejuvenation, which can be seen by their bluer positions near the TAMS and increased luminosity during post-MS evolution, they ignite helium and often complete helium burning as BSGs or YSGs. Therefore, Geneva models cannot explain the observed luminosity spread of RSGs in young open clusters. Similarly, Figure H2 shows that although rotational mixing leads to a luminosity spread among BSGs, it does not explain the luminosity spread of RSGs. In fact, Figure H2 shows that the Geneva models do not predict any RSGs at the ages corresponding to the observed clusters. This is because these models adopt a lower overshooting parameter

($\alpha_{\rm ov} = 0.1$) and the Schwarzschild criterion to determine the convective boundary, which favor the formation of BSGs over RSGs. To thoroughly investigate whether rotational mixing can lead to a luminosity spread among RSGs, further theoretical studies, incorporating varying parameters for internal mixing, are required.
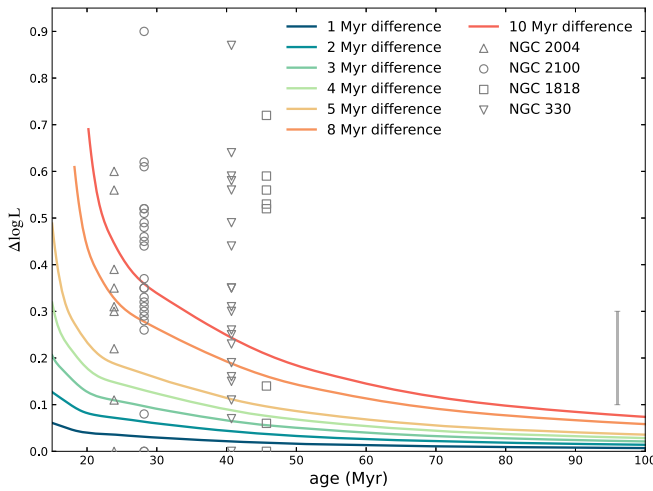
Appendix I
Impact of Real Age Difference

In this Appendix, we explore the impact of a potential real age difference on the luminosity of RSGs in young open clusters. It is important to note that current observations suggest that a significant real age difference among stars in young open clusters is unlikely. Observations indicate that stars in young open clusters have identical chemical compositions (A. Mucciarelli et al. 2014; A. P. Milone et al. 2016), suggesting that they belong to the same generation. Previous studies proposed extended star formation as a possible explanation for the extended MS turnoff observed in young open clusters (A. D. Mackey & P. Broby Nielsen 2007; P. Goudfrooij et al. 2014). P. Goudfrooij et al. (2014) found a mass threshold of approximately $10^{4.8} M_\odot$ above which clusters can retain stellar ejecta to form a second generation of stars. However, the extended MS turnoff feature has also been observed in clusters with significantly lower masses than this threshold. Notably, two clusters in this study (NGC 2004 and NGC 1818) that show a spread luminosity distribution of RSGs are also measured to be less massive than this threshold. Additionally, N. Bastian & J. Strader (2014) examined 13 young open clusters, including NGC 330 and NGC 1818, in the Magellanic Clouds and found no evidence of gas or dust within them, which argues against continuous star formation.

In Figure I1, we compare isochrones of different ages, derived from our single-star models, with the observed MS stars in NGC 330. To transform model temperatures and luminosities into colors and magnitudes, we used the method described in C. Wang et al. (2022). For this comparison, we adopted a distance modulus of 18.65 and reddening $E(B - V) = 0.07$, such that the 40 Myr isochrone best fits the majority of MS stars in NGC 330. Our results show that real
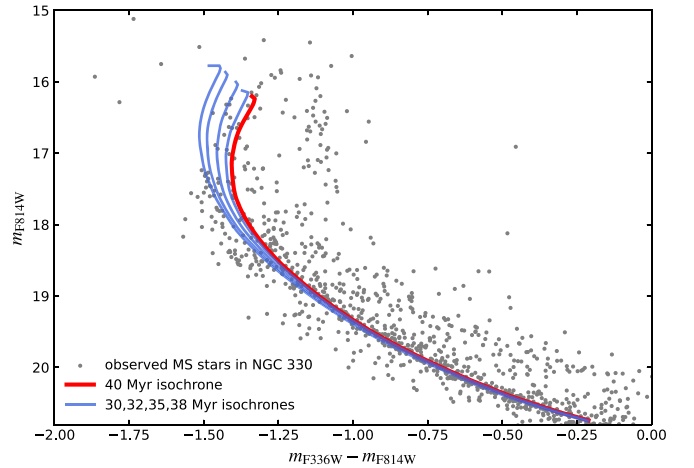
Figure I1. Impact of a real age difference on the distribution of MS stars in the color–magnitude diagram. The red line represents the 40 Myr isochrone from our single-star models with initial rotation rates of 55% of their breakup velocities. The blue lines correspond to the younger isochrones derived from these models, ranging from 30 to 38 Myr (from left to right). Observed MS stars in the cluster NGC 330 are overplotted as gray dots.

Figure I2. Luminosity difference of RSGs as a function of cluster age, caused by real age differences. At a given age, $\Delta \log L$ represents the difference between the baseline luminosity L_0 (see Appendix -Appendix link code C) at that age and the baseline luminosity at an age that is younger by specific values (ranging from 1 to 10 Myr), as shown by lines in different colors. The luminosity differences of observed RSGs relative to the least luminous RSG in four young open clusters are overplotted as open markers. Observational uncertainties are illustrated by the gray error bar in the lower right corner.

age differences cannot account for the blue MS stars fainter than approximately 18.5 mag, as unevolved MS stars exhibit nearly identical colors. Meanwhile, real age differences exceeding approximately 5 Myr cannot explain the observed distribution of MS turnoff stars. This is evident from the lack of stars on the 30 Myr and 32 Myr isochrones above 17.2 mag.

In Figure I2, we examine the impact of a real age difference on the luminosity extension of RSGs in young open clusters. The impact is more significant in younger clusters because at younger ages, a given age difference corresponds to a larger mass difference. For example, in a 25 Myr cluster, a 5 Myr age difference produces a luminosity difference of approximately 0.18 dex, while a 2 Myr difference results in a 0.06 dex luminosity spread. In contrast, these values decrease to 0.09 and 0.03 dex, respectively, in a 45 Myr cluster.

ORCID iDs

Chen Wang ● https://orcid.org/0000-0002-0716-3801
Lee Patrick ● https://orcid.org/0000-0002-9015-0269
Abel Schootemeijer ● https://orcid.org/0000-0002-2715-7484
Selma E. de Mink ● https://orcid.org/0000-0001-9336-2825
Norbert Langer ● https://orcid.org/0000-0003-3026-0367
Nikolay Britavskiy ● https://orcid.org/0000-0003-3996-0175
Xiao-Tian Xu ● https://orcid.org/0000-0001-9565-9462
Julia Bodensteiner ● https://orcid.org/0000-0002-9552-7010
Eva Laplace ● https://orcid.org/0000-0003-1009-5691
Ruggero Valli ● https://orcid.org/0000-0003-3456-3349
Alejandro Vigna-Gómez ● https://orcid.org/0000-0003-1817-3586
Jakub Klencki ● https://orcid.org/0000-0002-7527-5741
Stephen Justham ● https://orcid.org/0000-0001-7969-1569
Cole Johnston ● https://orcid.org/0000-0002-3054-4135
Jing-ze Ma ● https://orcid.org/0000-0002-9911-8767

References

Abt, H. A. 1983, ARA&A, 21, 343
Banyard, G., Mahy, L., Sana, H., et al. 2023, A&A, 674, A60
Bastian, N., & Lardo, C. 2018, ARA&A, 56, 83
Bastian, N., & Strader, J. 2014, MNRAS, 443, 3594
Beasor, E. R., & Davies, B. 2016, MNRAS, 463, 1269
Beasor, E. R., Davies, B., Smith, N., & Bastian, N. 2019, MNRAS, 486, 266
Beasor, E. R., Davies, B., Smith, N., et al. 2020, MNRAS, 492, 5994
Bellinger, E. P., de Mink, S. E., van Rossem, W. E., & Justham, S. 2024, ApJL, 967, L39
Braun, H., & Langer, N. 1995, A&A, 297, 483
Britavskiy, N., Lennon, D. J., Patrick, L. R., et al. 2019, A&A, 624, A128
Brott, I., de Mink, S. E., Cantiello, M., et al. 2011, A&A, 530, A115
Choi, J., Dotter, A., Conroy, C., et al. 2016, ApJ, 823, 102
Claret, A., & Torres, G. 2016, A&A, 592, A15
Davies, B., Kudritzki, R.-P., Plez, B., et al. 2013, ApJ, 767, 3
de Mink, S. E., Cantiello, M., Langer, N., et al. 2009, A&A, 497, 243
de Mink, S. E., Langer, N., Izzard, R. G., Sana, H., & de Koter, A. 2013, ApJ, 764, 166
Drout, M. R., Massey, P., Meynet, G., Tokarz, S., & Caldwell, N. 2009, ApJ, 703, 441
Ekström, S., Georgy, C., Eggenberger, P., et al. 2012, A&A, 537, A146
Eldridge, J. J., Beasor, E. R., & Britavskiy, N. 2020, MNRAS, 495, L102
Eldridge, J. J., Izzard, R. G., & Tout, C. A. 2008, MNRAS, 384, 1109
Farrell, E. J., Groh, J. H., Meynet, G., et al. 2019, A&A, 621, A22
Georgy, C., Ekström, S., Granada, A., et al. 2013, A&A, 553, A24
Glebbeek, E., Gaburov, E., Portegies Zwart, S., & Pols, O. R. 2013, MNRAS, 434, 3497
Goudfrooij, P., Girardi, L., Kozhurina-Platais, V., et al. 2014, ApJ, 797, 35
Gratton, R. G., Carretta, E., & Bragaglia, A. 2012, A&ARv, 20, 50
Guinan, E., Wasatonic, R., Calderwood, T., & Carona, D. 2020, ATel, 13512, 1
Haberl, F., & Sturm, R. 2016, A&A, 586, A81
Hastings, B., Langer, N., Wang, C., Schootemeijer, A., & Milone, A. P. 2021, A&A, 653, A144
Hellings, P. 1983, Ap&SS, 96, 37
Hobbs, G., Lorimer, D. R., Lyne, A. G., & Kramer, M. 2005, MNRAS, 360, 974
Justham, S., Podsiadlowski, P., & Vink, J. S. 2014, ApJ, 796, 121
Kee, N. D., Sundqvist, J. O., Decin, L., de Koter, A., & Sana, H. 2021, A&A, 646, A180
Kippenhahn, R., & Weigert, A. 1967, ZAp, 65, 251
Kiss, L. L., Szabó, G. M., & Bedding, T. R. 2006, MNRAS, 372, 1721
Korntreff, C., Kaczmarek, T., & Pfalzner, S. 2012, A&A, 543, A126
Kozai, Y. 1962, AJ, 67, 591
Li, C., de Grijs, R., Deng, L., & Milone, A. P. 2017, ApJ, 844, 119
Lidov, M. L. 1962, P&SS, 9, 719
Mackey, A. D., & Broby Nielsen, P. 2007, MNRAS, 379, 151
Maeder, A., & Meynet, G. 2000, ARA&A, 38, 143
Massey, P., Silva, D. R., Levesque, E. M., et al. 2009, ApJ, 703, 420
McLaughlin, D. E., & van der Marel, R. P. 2005, ApJS, 161, 304
Milone, A. P., Bedin, L. R., Piotto, G., & Anderson, J. 2009, A&A, 497, 755
Milone, A. P., Bedin, L. R., Piotto, G., et al. 2015, MNRAS, 450, 3750
Milone, A. P., Cordoni, G., Marino, A. F., et al. 2023, A&A, 672, A161
Milone, A. P., Marino, A. F., D'Antona, F., et al. 2016, MNRAS, 458, 4368
Milone, A. P., Marino, A. F., Di Criscienzo, M., et al. 2018, MNRAS, 477, 2640
Mucciarelli, A., Dalessandro, E., Ferraro, F. R., Origlia, L., & Lanzoni, B. 2014, ApJL, 793, L6
Narloch, W., Pietrzyński, G., Gieren, W., et al. 2021, A&A, 647, A135
Neo, S., Miyaji, S., Nomoto, K., & Sugimoto, D. 1977, PASJ, 29, 249
Niederhofer, F., Hilker, M., Bastian, N., & Silva-Villa, E. 2015, A&A, 575, A62
Offner, S. S. R., Moe, M., Kratter, K. M., et al. 2023, in ASP Conf. Ser. 534, Protostars and Planets VII, ed. S. Inutsuka et al. (San Francisco, CA: ASP), 275
Öpik, E. 1924, PTarO, 25, 1
Packet, W. 1981, A&A, 102, 17
Patrick, L. R., Evans, C. J., Davies, B., et al. 2016, MNRAS, 458, 3968
Patrick, L. R., Lennon, D. J., Evans, C. J., et al. 2020, A&A, 635, A29
Patrick, L. R., Lennon, D. J., Schootemeijer, A., et al. 2024, arXiv:2412.18554
Paxton, B., Bildsten, L., Dotter, A., et al. 2011, ApJS, 192, 3
Paxton, B., Cantiello, M., Arras, P., et al. 2013, ApJS, 208, 4
Paxton, B., Marchant, P., Schwab, J., et al. 2015, ApJS, 220, 15
Paxton, B., Schwab, J., Bauer, E. B., et al. 2018, ApJS, 234, 34
Pfahl, E., Rappaport, S., Podsiadlowski, P., & Spruit, H. 2002, ApJ, 574, 364
Podsiadlowski, P. 1992, PASP, 104, 717
Podsiadlowski, P., Langer, N., Poelarends, A. J. T., et al. 2004, ApJ, 612, 1044
Portegies Zwart, S. F., McMillan, S. L. W., & Gieles, M. 2010, ARA&A, 48, 431

Rocha, K. A., Kalogera, V., Doctor, Z., et al. 2024, ApJ, 971, 133
Salpeter, E. E. 1955, ApJ, 121, 161
Sana, H., de Mink, S. E., de Koter, A., et al. 2012, Sci, 337, 444
Schneider, F. R. N., Podsiadlowski, P., Langer, N., Castro, N., & Fossati, L. 2016, MNRAS, 457, 2355
Schneider, F. R. N., Podsiadlowski, P., & Laplace, E. 2024, A&A, 686, A45
Schootemeijer, A., Langer, N., Grin, N. J., & Wang, C. 2019, A&A, 625, A132
Sen, K., Langer, N., Marchant, P., et al. 2022, A&A, 659, A98
Shao, Y., & Li, X.-D. 2014, ApJ, 796, 37
Shenar, T., Sana, H., Mahy, L., et al. 2022, A&A, 665, A148
Smith, N. 2014, ARA&A, 52, 487
Soraisam, M. D., Bildsten, L., Drout, M. R., et al. 2018, ApJ, 859, 73
Tokovinin, A., & Moe, M. 2020, MNRAS, 491, 5158

Vinciguerra, S., Neijssel, C. J., Vigna-Gómez, A., et al. 2020, MNRAS, 498, 4705
von Zeipel, H. 1910, AN, 183, 345
Wang, C., Bodensteiner, J., Xu, X.-T., et al. 2024, ApJL, 975, L20
Wang, C., Hastings, B., Schootemeijer, A., et al. 2023, A&A, 670, A43
Wang, C., Langer, N., Schootemeijer, A., et al. 2020, ApJL, 888, L12
Wang, C., Langer, N., Schootemeijer, A., et al. 2022, NatAs, 6, 480
Wood, P. R., Bessell, M. S., & Fox, M. W. 1983, ApJ, 272, 99
Yang, M., Bonanos, A. Z., Jiang, B.-W., et al. 2018, A&A, 616, A175
Yang, M., Bonanos, A. Z., Jiang, B., et al. 2023, A&A, 676, A84
Yoon, S.-C., & Cantiello, M. 2010, ApJL, 717, L62
Zapartas, E., de Mink, S. E., Justham, S., et al. 2019, A&A, 631, A5
Zapartas, E., de Wit, S., Antoniadis, K., et al. 2024, arXiv:2410.07335